Park *et al. Journal of Nanobiotechnology* (2025) 23:285
https://doi.org/10.1186/s12951-025-03351-9

Journal of Nanobiotechnology

REVIEW Open Access

Nanodiamond: a multifaceted exploration of electrospun nanofibers for antibacterial and wound healing applications

Hyeonseo Park[1,2†], Tejal V. Patil[1,2†], Changyeun Mo[1,2*] and Ki-Taek Lim[1,2,3*]

Abstract

In this review, we explore the exciting potential of nanodiamonds (NDs) as innovative materials for future wound dressings. These materials aim to tackle important issues in wound care and offer fresh solutions. While NDs show promising mechanical and structural properties, their full potential in wound healing applications is still not fully explored. We emphasize their unique features—like high surface area, the dispersion of functional groups, and excellent purity—which contribute to their mechanical stability, adhesion, growth, and movement—all critical for effective wound healing and tissue repair. We also focused on modifying the surface of these particles using various functionalization, which can enhance their biocompatibility, antibacterial properties, heat conductivity, and wettability. This positions NDs as a powerful tool for improving chronic wound care in the future. However, there are notable challenges when it comes to scaling up ND-based nanofiber matrices, which currently limits the electrospinning process for mass production. Also, issues with the physical and chemical stability of ND-based nanofibers when interacting with cells need to be resolved to guarantee long-lasting effectiveness. In this study, we tackle these challenges by suggesting solutions like surface functionalization, optimizing the electrospinning process, and creating hybrid scaffolds. Our findings show that these innovations can effectively address scalability and stability issues, paving the way for broader clinical applications. This review not only emphasizes the advantages of NDs in wound healing but also introduces new insights for enhancing the biocompatibility and functionality of ND-based nanofibers, finally pushing the technology of wound dressings forward.

[†]Hyeonseo Park and Tejal V. Patil contributed equally to this work.

*Correspondence:
Changyeun Mo
cymoh100@kangwon.ac.kr
Ki-Taek Lim
ktlim@kangwon.ac.kr
[1]Department of Biosystems Engineering, Kangwon National University, Chuncheon, Gangwon-do 24341, Republic of Korea
[2]Interdisciplinary Program in Smart Agriculture, Kangwon National University, Chuncheon, Gangwon-do 24341, Republic of Korea
[3]Institute of Forest Science, Kangwon National University, Chuncheon, Gangwon-do 24341, Republic of Korea

Graphical Abstract

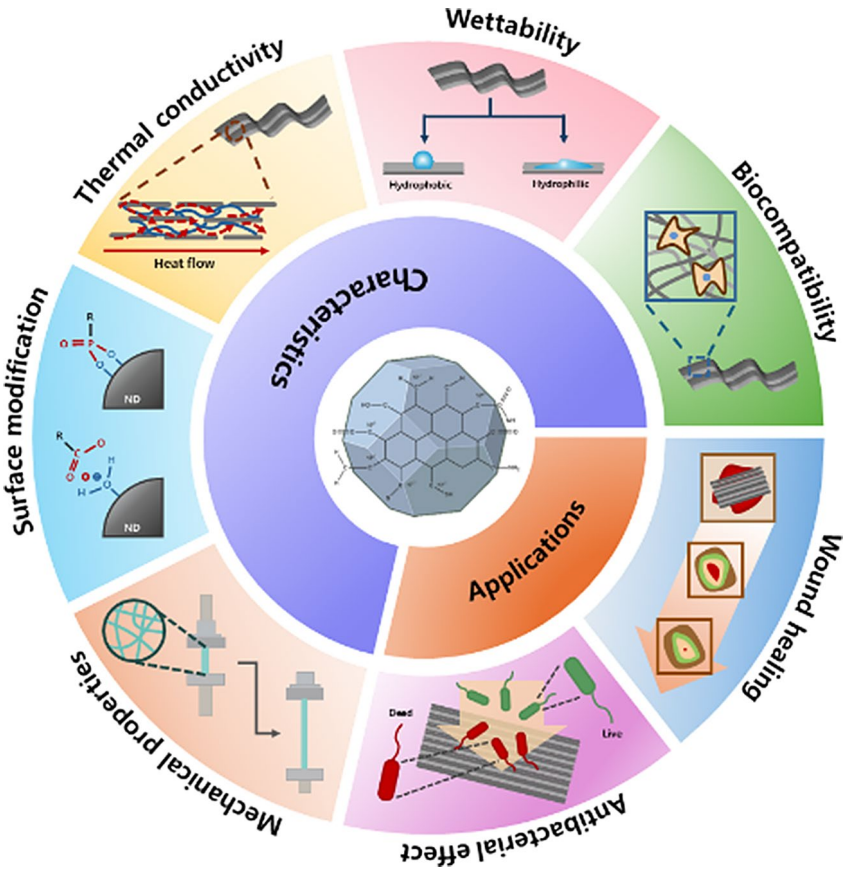

Keywords Nanodiamond, Nanofiber, Surface modification, Antibacterial, Biocompatibility, Wound healing

Introduction

Nanodiamonds (ND) have gathered significant attention in recent years as a versatile and high-throughput nanomaterial with immense potential in biomedical applications [1, 2]. These carbon-based nanoparticles are typically ranging in size from 2 to 5 nm and are synthesized using detonation or high-pressure high-temperature (HPHT) methods. Structurally they exhibit a unique core-shell architecture with an sp^3-bonded carbon core resembling a diamond and an outer shell composed of graphitic or amorphous carbon layers [3]. This dual structure imparts NDs with a combination of diamond-like properties such as exceptional hardness and high thermal conductivity and surface versatility, enabling chemical modifications that extend their applications across diverse fields. One of the defining features of NDs is their highly functionalizable surface, which can be modified with a range of chemical groups, including carboxyl, hydroxyl, amine, and halogen functionalities [4, 5]. These surface modifications improve their dispersion in polar and nonpolar solvents, enhance their compatibility with biological systems, and enable targeted interactions. The ability to tailor their surface chemistry allows NDs to serve as carriers for drug delivery, improve the mechanical properties of composite materials, and provide antibacterial and antioxidant functionalities. Furthermore, NDs exhibit excellent biocompatibility, chemical inertness, and a low risk of cytotoxicity, making them ideal for applications in sensitive biological environments [6]. Beyond their structural and chemical adaptability, NDs possess superior mechanical properties such as high tensile strength and durability. This make them an excellent reinforcing agent for polymers and nanofibers [7]. The high thermal conductivity allows for efficient heat management while their surface energy can be tuned to optimize wettability, enabling the control of moisture in biomedical applications [8]. These unique properties position NDs as a key component in designing advanced materials for tissue engineering, drug delivery and regenerative medicine.

As already discussed, NDs have immense applications in biomedical field. Rather than utilizing NDs in their

intrinsic nanoparticle form, they are often integrated into scaffolds, which can further enhance their properties. Nanodiamond incorporated scaffolds presents considerable promise for advancement of regenerative medicine and improving patient outcomes [9]. In this context, scaffolds in nanofibrous structures play a crucial role in biomedical applications due to their structural similarity to extracellular matrix, which supports cell attachment and growth [10]. Electrospinning is a powerful technique that uses electrostatic forces to fabricate nanofibers from polymer solutions [11]. The structural arrangement has significance in biomedical applications, particularly wound healing, due to their potential to replicate the native extracellular matrix (ECM), an essential factor to promote tissue regeneration [12]. The high surface area to volume ratio of nanofibers enhances nutrient release, promoting adhesion, proliferation and faster healing of wounds along with sustained release of bioactive molecules. These nanofibers can be fabricated in numerous patterns including core-shell [13], hollow, coaxial [14], bilayer [15, 16], multilayer [17, 18], mesoporous and solid nanofibers which can be used as per the desired applications. The flexibility of this technique allows researchers use different polymers and add therapeutic agents, making it a breakthrough in advanced wound care [13, 14]. Hence, the integration of nanostructured nanomaterials into electrospun nanofibers has opened new avenues to addressing challenges in wound healing, a critical area of biomedical research [9]. Wound healing is a multifaceted process that involves hemostasis, inflammation, proliferation and remodeling which can be hindered by factors such as bacterial infections, excessive inflammation and poor tissue regeneration [19]. Chronic wounds represent a considerable healthcare burden due to their prolonged healing times and susceptibility to infections. Electrospun nanofibers mimic the architecture and function of the extracellular matrix (ECM), provide a promising platform for wound care by promoting cell adhesion, migration and proliferation. Incorporating NDs into these nanofibers not only enhances their structural integrity and mechanical properties but also imparts multifunctional capabilities such as antibacterial properties, thermal stability and controlled drug delivery. One of the most significant contributions of ND-based nanofibers in wound healing is their ability to combat bacterial infections [20]. NDs exhibit intrinsic antibacterial properties, disrupting bacteria membranes and inhibiting biofilm formation. Surface modifications further amplify these effects enabling the generation of reactive oxygen species (ROS) and enhanced interaction with bacterial cell walls [21]. In addition to their antibacterial properties, ND-based membranes maintain an optimal moisture balance at the wound site, preventing desiccation while minimizing the risk of excessive exudate accumulation [22]. This dual action fosters a conducive environment for tissue regeneration and accelerates the healing process. Moreover, biocompatibility of NDs ensures that their incorporation into wound dressings and scaffolds does not provoke adverse immune responses. The nanostructured surfaces of ND-infused nanofibers mimic the natural ECM providing a scaffold that supports the attachment and proliferation of key cell types involved in wound healing such as fibroblasts and keratinocytes [22]. The thermal and mechanical stability of these nanofibers further enhances their durability and makes them suitable for prolonged use in wound management.

In this review, we conduct a systematic examination of the synergistic promise of nanodiamonds (NDs) and electrospun nanofibers for wound healing and antibacterial applications. Our key aim is to define the structure-property relationships of ND and ND-reinforced nanofibers, with particular attention to how surface modifications affect their mechanical, thermal, and biological functionality. We also provide an in-depth discussion of NDs' inherent antibacterial properties, their capacity for moisture management, and their application in promoting tissue regeneration in electrospun scaffolds. Through the critical summary of recent advances and the description of current limitations, this review aims to provide a clear guideline for the development of next-generation wound dressing materials. We hope to contribute to the field by offering a panoramic overview of the existing knowledge, outlining key areas of knowledge gap, and proposing possible research avenues for the expediation of clinical translations of ND-based nanofibers. The organizational framework of this review is presented schematically in Scheme 1, serving as a visual representation of the manuscript.

Structure of ND

The properties of ND arise from the unique characteristics of both diamonds and nanoparticles [23]. The size of ND is generally in the range of 2–5 nm in size, with the most stable size considered to be 4–5 nm [24]. They are composed of sp^3 carbon atoms with structural properties similar to diamonds [25]. The structure of ND is characterized by a core-shell design, which can be divided into the core, intermediate layer, and surface layer. This structure has significant implications for the functionalization and applications of ND [26]. The core, measuring 2 ~ 3nm is composed of a lattice of sp^3-bonded carbon atoms and contains about 70–90% of the total carbon atoms. The sp^3 bonds are stable and inert, forming a core structure with low reactivity. However, various chemical groups can be attached to the outer surface of ND, making it highly biocompatible and suitable for use as a biomaterial. The intermediate layer is a nonhomogeneous transitional carbon shell with a thickness ranging from 0.4 to 1.0 nm. The

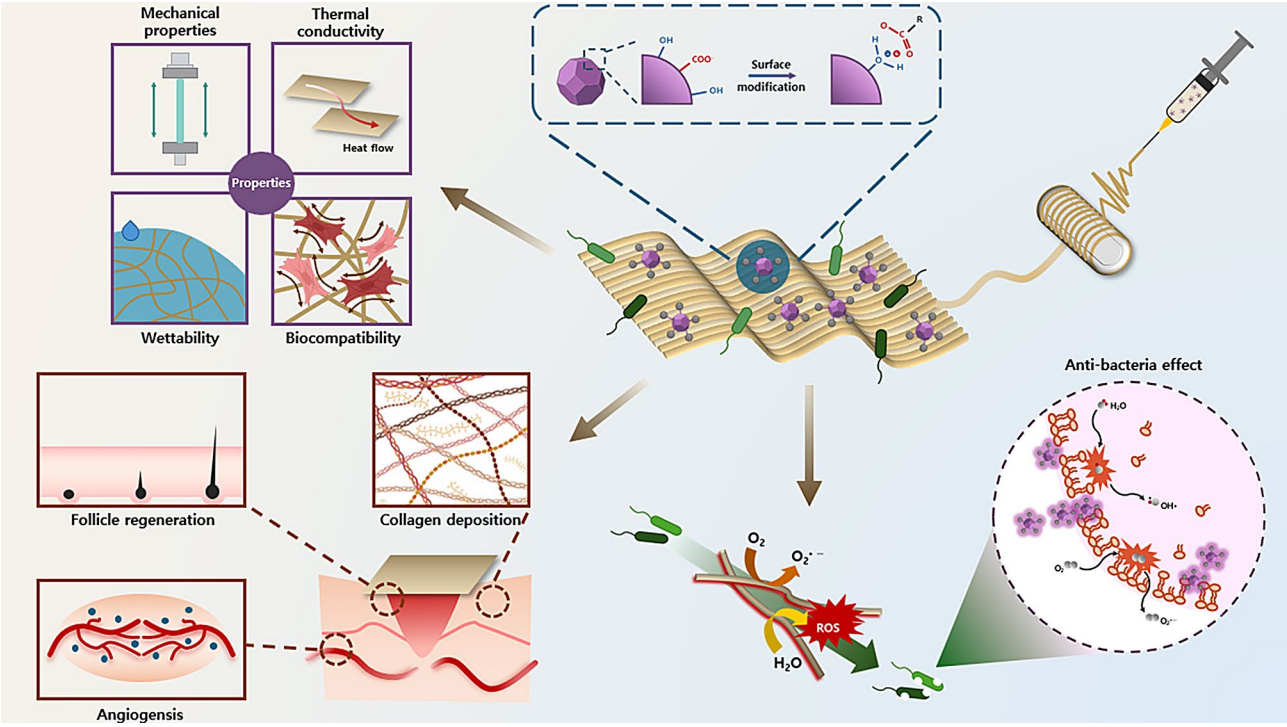

Scheme 1 ND-embedded nanofibers enhance mechanical and biological properties, promote antibacterial effects, angiogenesis, and collagen deposition, effectively supporting wound healing

inner surface of the shell is made up of continuous onion-like carbon (OLC) layers, while the outer surface consists of a single layer of graphitic carbon. Although the exact nature of the outer surface has not been fully elucidated, two general models have been proposed. One suggests an amorphous shell with significant sp^2 carbon content, while the other describes a 'bucky-diamond', which consist of sp^2 graphene sheets arranged in a fullerene-like structure [27]. These two types of bonds are interchangeable: the stretched face of a diamond can become a graphene plane, while puckered graphene can transform into a diamond surface. This interchangeability allows ND particles to act flexibly, especially around curved surfaces where electrons are unstable. The sp^2-bonded portion of the shell is useful for binding drugs or therapeutic agents, and in drug delivery systems, ND can efficiently encapsulate or target drugs [28]. In addition to carbon, the surface of ND contains atoms like oxygen, hydrogen, and nitrogen. ND also include small amounts of carboxylic acid groups, anhydrides, hydroxyl groups, and epoxide groups. Due to the presence of carboxyl groups, ND solutions maintain stability in water [23, 29]. The surface of ND can be modified with various functional groups and atoms, such as carboxyl groups, hydroxyl groups, hydrogen atoms, amide groups and halogen atoms, providing additional stability [30]. The surface functionalization of NDs with their change in properties and effects is described in detail in Sect. 3.2.

Characteristics of ND

ND not only possesses the properties of diamond but also exhibits characteristics of nanomaterials. It has excellent mechanical properties, high thermal conductivity, and a large surface area. Additionally, it features a tunable surface structure and outstanding biocompatibility [31, 32]. Furthermore, it has various distinctive characteristics, which are detailed below.

Mechanical properties

The carbon atoms present within the structure of ND are relatively small and lightweight, with short bond ranges within lattice. These bonds are very strong due to the covalent bonding associated with sp^3 hybridized tetrahedral structure, which contributes to the excellent mechanical properties of ND [33]. Mechanical properties can be measured through indicators such as tensile strength, elongation at break, Young's modulus, and abrasion resistance [34]. The superior mechanical properties of ND are transferred to other materials when combined with them. As a result, various polymer composites containing ND can exhibit significantly improved mechanical properties compared to pure polymers [35, 36]. For instance, in a study performed by Adhikari et al., polymer-nanodiamond fiber composites were fabricated using carboxylated ND (cND) (Fig. 1A-a) using poly(vinyl alcohol) (PVA), polyacrylonitrile (PAN), and polystyrene (PS). As illustrated in the Fig. 1A-b, the tensile strength

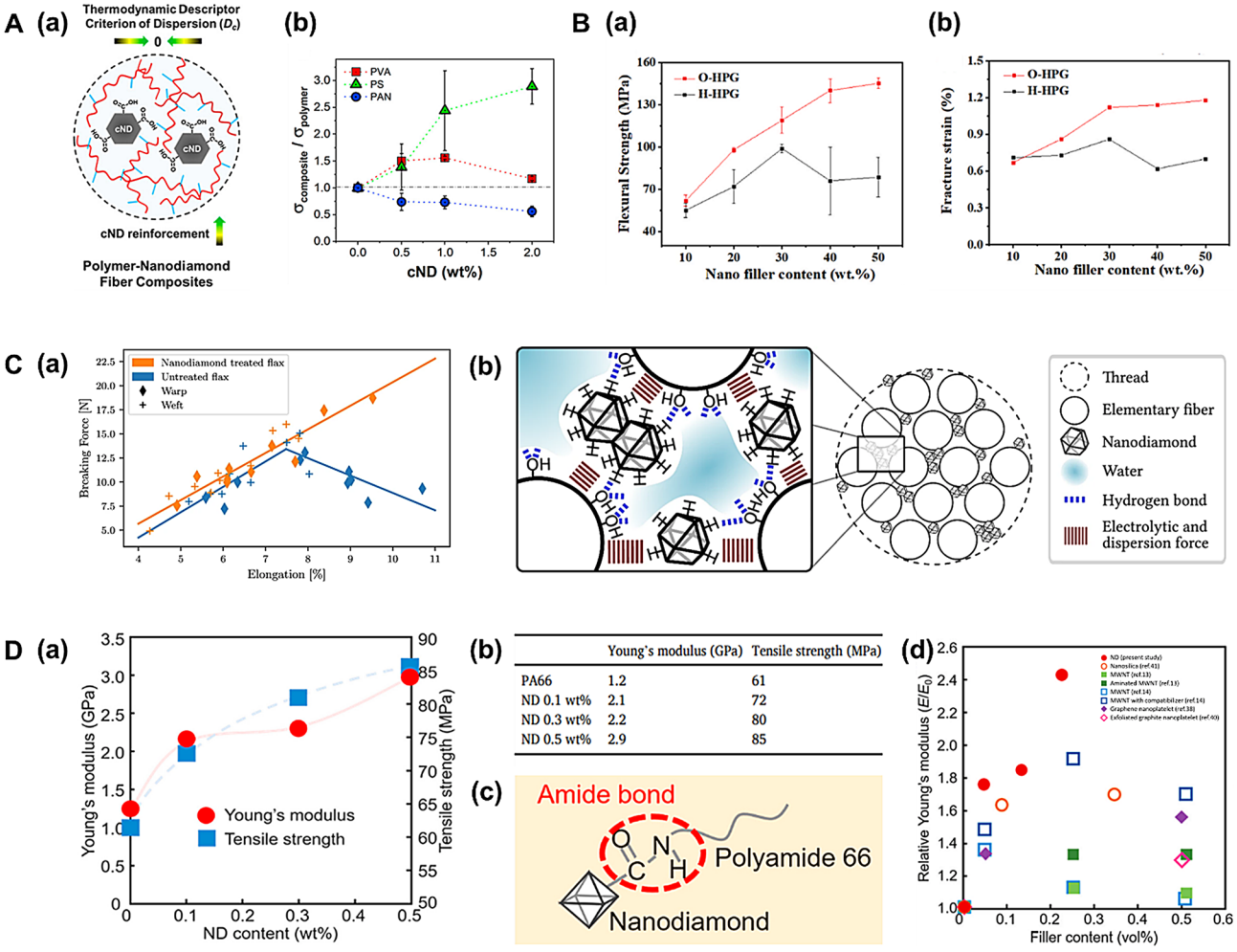

Fig. 1 (**A**): (a) Structure of polymer-ND fibers composites fabricated using cND. (b) Tensile strength of PVA, PS, and PAN as a function of cND content. Reproduced with permission [37]. (**B**): Mechanical properties of O-HPG and H-HPG for (a) Flexural strength (b) Fracture strain. Reproduced with permission [38]. (**C**): (a) Tensile strength at break as a function of elongation for untreated flax and ND treated flax (b) A cross-sectional schematic of flax fibers. Reproduced with permission [39]. (**D**): (a) Graph of the Young's modulus and tensile strength of ND content (b) Quantified values of Young's modulus and tensile strength of PA66 and PA66/ND. (c) Schematic diagram of the bonding between ND and PA66. (d) Graph of the relative Young's modulus of PA66 nanocomposites reinforced with ND, nanosilica, MWNT, and graphene nanoplatelets. Reproduced with permission [40]

measurements for each nanofiber demonstrated that the tensile strength of PS and PVA nanofibers exhibited an increasing trend with higher loading of cND, in comparison to samples without any cND incorporation. Notably, normalized tensile strength of PS exhibited the highest increase, with its value rising from 1 (cND wt% 0) to 2.84 (cND wt% 2.0) [37]. Similarly, Junzhuo et al. fabricated an electrospun polyacrylonitrile (PAN)-based superfine fiber reinforced with 75wt% ND to create O-HPG (high-performance graphite). In contrast, the control group, H-HPG, was produced using a particle reinforcement method. The mechanical properties of H-HPG and O-HPG showed that as the mass fractions of ND and PAN increased, the flexural strength and Young's modulus tended to increase. Overall, O-HPG demonstrated an average flexural strength that was 31% higher than that of H-HPG (Fig. 1B-a). Furthermore, as shown in the Fig. 1B-b, O-HPG exhibited a higher fracture strain compared to H-HPG having a maximum fracture strain of only 0.86%, while O-HPG reached 1.18% [38]. Hinzmann et al. produced untreated flax fibers (F) and ND-treated flax fibers (F_{ND}). The breaking force measurements revealed that the F exhibited a value of 10 ± 3 N, while F_{ND} showed a higher value of 12 ± 4 N compared to F. The tensile strength at break as a function of elongation was also measured, and F_{ND}'s breaking force consistently increased with elongation, showing higher values than F at almost all elongation points (Fig. 1C-a). The improvement in mechanical properties upon ND treatment is attributed to the enhanced cohesion between the individual flax fibers, as ND bind to the flax fibers, increasing the inter-fiber cohesion, as shown in the

Fig. 1C-b [39]. Morimune-Moriya et al. reported on the mechanical reinforcement effect of ND in polyamide 66 (PA66) nanocomposites. They demonstrated that incorporating only 0.5wt% ND led to a significant increase in Young's modulus and tensile strength, with improvements of 140% and 39%, respectively (Fig. 1D-a and b). This remarkable enhancement is attributed to the strong interactions between ND and PA66, including hydrogen bonds and amide bonds, as well as the uniform dispersion of ND within the PA66 matrix (Fig. 1D-c). Additionally, Fig. 1D-d compares the relative Young's modulus of PA66 nanocomposites reinforced with ND, nanosilica, MWNTs, and graphene nanoplatelets, showing that PA66/ND composites exhibited superior mechanical improvements even at lower filler contents compared to other composites [40]. This suggests that ND incorporated composites enhances the mechanical properties. However, it is crucial that the mechanical properties of these composites or nanofibers align with the mechanical properties of human skin for wound healing application. Skin is a viscoelastic material, meaning it exhibits both elastic and viscous behavior. Also, the Young's modulus of skin varies widely from 4 kPa to 140 MPa, depending upon factors like part of body, age and hydration [41]. For instance, nanofibers with tensile strength comparable to that of skin are likely to be more advantageous for wound healing applications. For example, Mahdavi and team found that addition of 1wt% ND particles in cellulose chitosan nanofibers, increased the elastic modulus and yield strength of fibers, which was close to the natural skin [42]. However, high ND (3wt%) decreased the durability of fibers. Their respective cell viability results showed that compared to high ND, low ND incorporated nanofibers showed more biocompatibility. Another group showed the effect of ND (0.5, 1, 2 and 3wt%) with PLA [43]. 1wt% ND showed highest Young's modulus (9.95 ± 1.25), tensile strength (1.12 ± 0.14) among all the compositions. Compared to neat PLA nanofibers, the increased value was 161% in Young's modulus and 239% in tensile strength. The PLA/ND was further studied for cell adhesion [44]. Notably, PLA matrices containing lower ND concentrations (0.1 and 0.5 wt%) exhibited significantly enhanced L929 cell adhesion compared to neat PLA, indicating the potential of these concentrations to improve cellular support. Furthermore, cell spreading was observed to be superior in the 0.1 and 0.5 wt% ND composites compared to those with 1 wt% ND. These findings suggest an inverse correlation between nanofiber mechanical properties and cellular adhesion and migration. Consequently, a systematic optimization of ND concentration is imperative to modulate nanofiber tensile strength, achieve congruence with the physiological mechanical properties of native skin, and thoroughly evaluate their biological efficacy.

Surface modification

ND surfaces not only expand but also possess adjustable properties [45]. Most commercially available ND surfaces contain various functional groups such as carboxyl, hydroxyl, lactone, and ketone, leading to a high degree of oxidation [46]. The presence of these groups, along with sp^2 carbon, directly affects the stability of ND particles, making them prone to agglomeration into larger aggregates [47]. Therefore, it is necessary to modify the surface groups of ND. Surface modification also plays an important role in increasing solubility in various polar organic solvents, improving stability, and cellular adhesion. For example, oxygen terminated NDs show high cellular attachment than hydrogen terminated NDs [48]. Additionally, it enhances biocompatibility and reduces toxicity [4, 23]. Surface modification can be achieved through mechanical and chemical methods. Mechanical methods include ultrasonic treatment and ball milling, while sonication using ceramic beads and subsequent ultrasonic techniques are also applicable. Chemical methods include heating ND powder in air at 400–430 °C to remove sp^2 carbon impurities [49, 50]. Due to the chemical versatility of ND, surface chemistry can be tailored to various environments using organic chemical transformations [51]. The common chemical transformations applied to the ND surface are described in detail Fig. 2 and below. Additionally, the advantages and disadvantages of each surface modification method are listed in Table 1.

Carboxylation

During the production of ND, the surface can become contaminated with sp^2 carbon structures and metallic impurities [58].To remove these, oxidative treatments using air, ozone-enriched air, or acids are carried out, ideally resulting in the formation of carboxyl groups (-COOH) on the ND surface. Strong acids such as nitric acid (HNO_3), hydrochloric acid (HCI), perchloric acid ($HCIO_4$), and sulfuric acid (H_2SO_4), along with oxidizing agents like potassium nitrate (KNO_3) and potassium dichromate ($K_2Cr_2O_7$), can oxidize the carbon on the ND surface, forming carboxyl groups [38]. Additionally, air or ozone air treatment at high temperatures in an eco-friendly and cost-effective method for removing surface impurities while generating carboxyl groups [59]. The carboxyl groups formed on the ND surface contribute to expanding potential applications in various fields by introducing oxygenated groups onto the surface.

Li et al. synthesized a polyvinylidene fluoride-carboxylated nanodiamond/titanium dioxide (PVDF-CND/TiO_2) composite. The introduction of carboxyl groups on the ND surface significantly improves the dispersion of ND, which in turn enhances the interaction with TiO_2 particles. As a result, the hydrophilicity of the membrane increases, leading to substantial improvements in

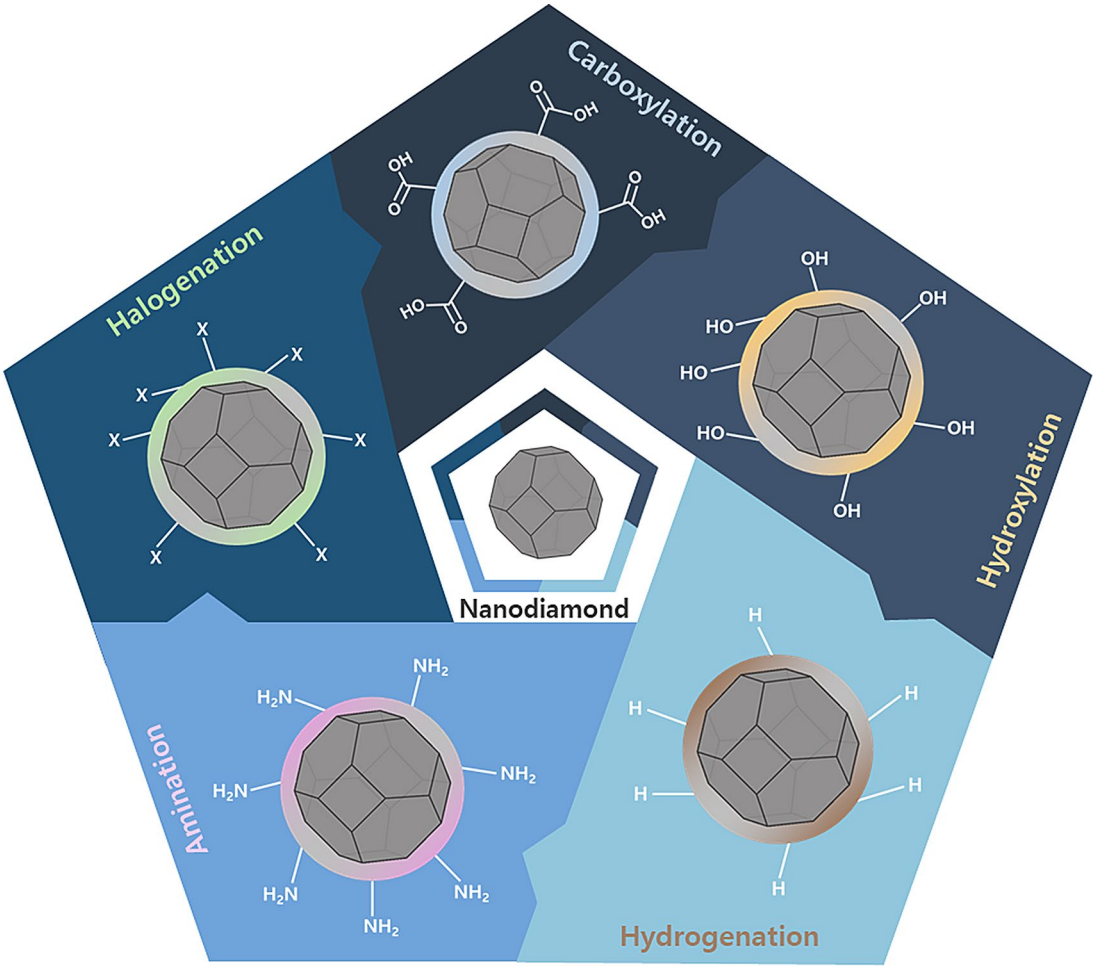

Fig. 2 Schematic representation of functionalization of ND surfaces

antifouling and self-cleaning properties (Fig. 3A) [60]. Yang et al. functionalized nanodiamond by adding carboxyl groups. They then attached mCherry protein to the ND and covalently bonded linear DNA-encoding components of the CRISPR-Cas9 system, which included an homology-directed repair (HDR) template, sgRNA, Cas0 protein, and a green fluorescent protein (GFP) reporter. This ND-based delivery system is not only capable of being internalized by the mouse retina but can also introduce X-linked retinoschisis (XLRS)-specific mutations in the *RS1* gene [61]. Hou et al. synthesized carboxylated ND (ND-COOH) by annealing pristine ND. Subsequently, ND- PEI was further prepared by grafting ethylenediamine-branched polyethylenimine onto ND-COOH demonstrated a photothermal conversion efficiency of approximately 20% under 808 nm NIR irradiation, exhibiting stable photothermal properties. Additionally, in in vitro antibacterial experiments, ND-COOH at concentrations of 150 μg/mL and 200 μg/mL co-cultured with *E. coli* and *S. aureus*, respectively, led to over 99% bacterial eradication after 10 min of NIR irradiation in both cases. This indicates that the functional groups enhance antibacterial activity, making it beneficial for bacterial infection treatment (Fig. 3B) [62]. Zandieh et al. evaluated the potential of carboxylated, hydroxylated, and hydrogenated ND (COOH-ND, OH-ND, H-ND) as biosensors for DNA detection by desorbing pre-absorbed FAM-labeled DNA using complementary DNA (cDNA). The DNA detection process is illustrated in Fig. 3C-a. To assess specificity, they added FAM-unlabeled DNA (rDNA) separately. The specificity factors for COOH-ND, OH-ND, H-ND, and GO were calculated as 3.0, 1.9, 0.9, and 2.5, respectively, with COOH-ND showing the highest specificity. In contrast, H-ND failed to distinguish between cDNA and rDNA (Fig. 3C-b). Additionally, by adding various concentrations of cDNA to FAM-DNA pre-absorbed on COOH-ND, a correlation was observed where fluorescence enhancement increased with cDNA concentration (Fig. 3C-c). This suggests that COOH-ND can enable quantitative measurement of DNA concentration in unknown samples and facilitate DNA detection [63]. Moreover, it implies that COOH-ND can be

Table 1 Advantages and disadvantages of different surface modifications of ND

Surface modifications	Advantages	Disadvantages	Ref
Carboxylation	- Improves hydrophilicity and dispersion in water - Non cytotoxic - Biocompatible - Antioxidant properties	- Presence of many impurities and lattice defects - May reduce thermal properties due to oxygen functional groups - Environmental and handling problems due to strong acid use	[52, 53]
Hydroxylation	- Help with continuous drug release - Enhanced biocompatibility - Increased water solubility - Facilitates further functionalization	- Presence of impurities - Complex process control	[33]
Hydrogenation	- Restores diamond-like properties (high thermal stability, hardness) - Improves surface energy for specific bonding applications - High reactivity to oxygen species	- Limited stability in air - Increased hydrophobicity reduces drug solubility and release capacity	[34]
Amination	- Excellent biocompatibility - Enhances compatibility with polymers for composite materials - Provides functional groups for bioconjugation and drug delivery systems	- May introduce cytotoxicity if not purified properly - Possession of complex structure - Non-uniform surface reactivity	[54, 55]
Halogenation	- Improved thermal stability - Increased hydrophobicity - Enhanced chemical reactivity	- Degradation of biocompatibility - Complex processing - Low productivity	[56, 57]

effectively used to monitor important cellular and tissue responses in the wound healing process and quickly diagnose infections occurring at the wound site. ND possess numerous outstanding properties, but oxygen-containing functional groups can lead to strong inter-particle attraction, causing agglomeration. This agglomeration significantly reduces the reinforcement potential of ND within the matrix [6, 64]. To address this issue, Shuai et al. utilized phospholipids (PL). The hydroxyl group (-OH) on the PL head forms hydrogen bonds with the carboxyl group (-COOH) on the surface-modified ND, aligning the PL tails toward the poly-l-lactic acid (PLLA) matrix (Fig. 3D-a). Consequently, ND particles are enveloped by a PL layer, with repulsion between the tails keeping them separated, thereby enhancing ND dispersion in PLLA. The resulting PLLA/ND-PL composites showed higher cell density of MG-63 human osteosarcoma (MG63) cells after 5 days compared to PLLA, with cells progressively developing filopodia and lamellipodia (Fig. 3D-b, c, d, and e). This indicates that PLLA/ND-PL possesses superior cytocompatibility, promoting cell proliferation more effectively than PLLA [65].

Hydroxylation

The hydroxylation of ND is one of the most commonly used surface modification methods due to its potential for various subsequent reactions. The hydroxylation of the ND surface can be achieved through reduction with lithium aluminum hydride ($LiAlH_4$) or borane (BH_3·THF) [66, 67]. Additionally, the Fenton reaction (a solution of $FeSO_4$ with H_2O_2) is an efficient method for generating -OH groups [68, 69]. Mechanochemical treatments and photochemical methods involving UV irradiation in the presence of O_2 and H_2O are also included in hydroxylation processes. UV irradiation generates atomic oxygen and OH radicals, which not only create terminal -OH groups on the ND surface but also remove other oxygenated surface functional groups [48].

Zhong et al. prepared ND with carboxyl groups (-COOH) reduced to hydroxyl groups using sodium borohydride ($NaBH_4$) as a reducing agent through a mechanochemical modification method (Fig. 4A-a). As shown in the Fig. 4A-b, the evaluation of the oil-saving performance of ND-based lubricating oil revealed that the average fuel consumption rate of PAO6 without ND was 7.225 L/100km. In contrast, PAO6 containing 0.02% ND surface-modified with hydroxyl groups demonstrated an average fuel consumption rate of 6.667 L/100 km, representing a 7.72% reduction in fuel consumption. This indicates that surface-modified ND has potential as a lubricant additive, contributing to energy savings [70]. Lim et al. developed a hyaluronic acid (HA)/ND 3D printed nanocomposite hydrogel using hydroxylated ND (Fig. 4B-a). They measured compressive mechanical stress at different pH levels, finding that at pH 7, the HA/ND-COOH exhibited a stress of 152.82 kPa, while the HA/ND-OH showed a higher value of 161.59 kPa (Fig. 4B-b). As shown in the Fig. 4B-c, at pH 8, the HA/ND-COOH had values of 168.31 kPa and 449.59 kPa for compositions of 0.02wt% and 0.04wt%, respectively. In contrast, the HA nanocomposite hydrogel containing ND-OH demonstrated values of 236.18 kPa and 616.72 kPa for the same compositions, indicating an increase of 1.4 times and 1.37 times compared to ND-COOH. This suggests that the use of hydroxylated ND enhances the mechanical properties even at low weight ratios [71]. This suggests the potential of hydroxylated ND in enhancing the performance for biomedical applications such as wound healing.

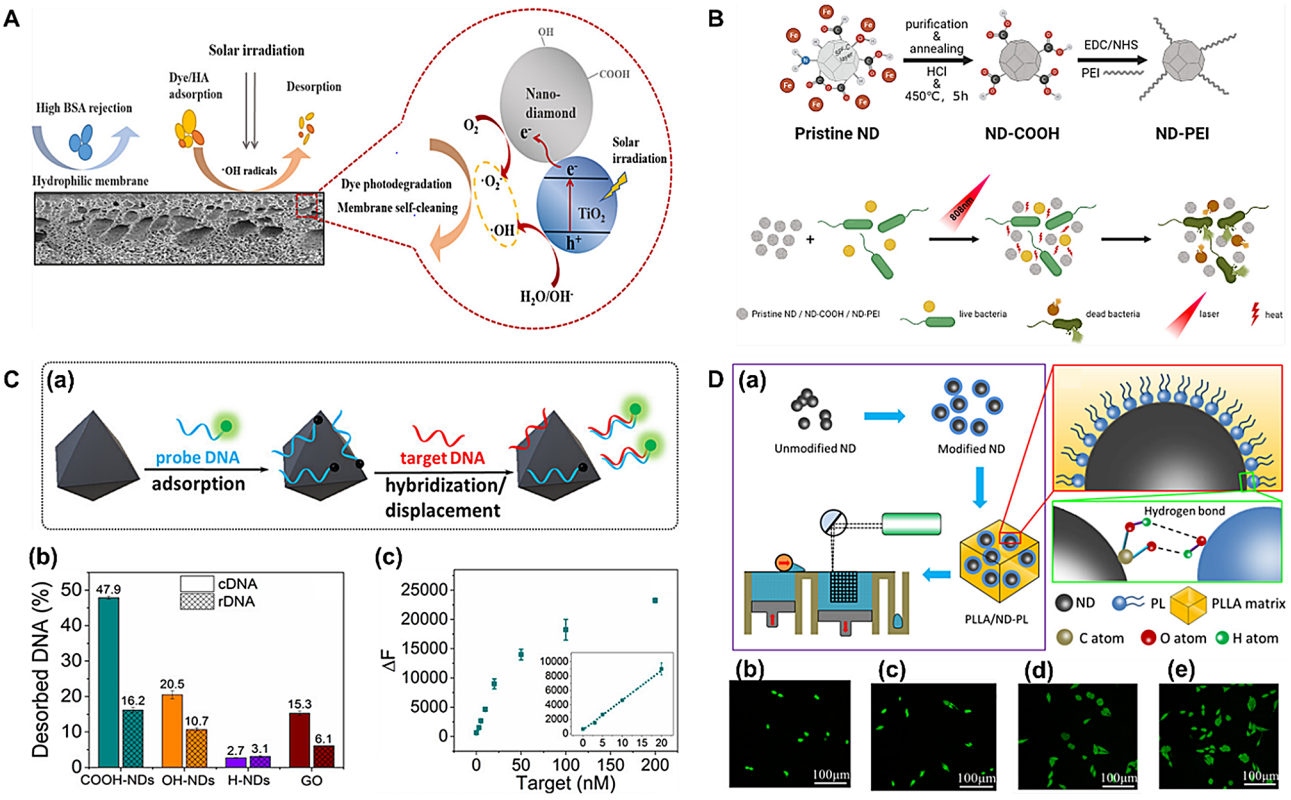

Fig. 3 (**A**) Schematic of anti-pollution and self-cleaning characteristics enhanced by CND composite. Reproduced with permission [60]. (**B**) Schematic of the synthesis process of ND-COOH and ND-PEI and their antibacterial properties under NIR irradiation. Reproduced with permission [62]. (**C**): (a) Schematic of the DNA detection process. (b) Comparison graph of fluorescence enhancement of COOH-ND, OH-ND, H-ND, GO when cDNA and rDNA are added. (c) Calibration curve of COOH-ND. Reproduced with permission [63]. (**D**): (a) Schematic diagram illustrating the fabrication of PLLA/ND-PL and the binding mechanism of ND-PL. Fluorescent staining images of MG63 cells incubated for (b) 1 day (c) 5 days in PLLA and (d) 1 day (e) 5 days in PLLA/ND-PL. Reproduced with permission [65]

Chi et al. used ND with -OH groups formed on their surface through a detonation synthesis process. After grafting dopamine polymer chains onto the ND surface, forming PDA-ND, perfluoroalkyl trimethoxysilane was modified to the side end of the dopamine polymer chain to create F-ND (Fig. 5A-a). Subsequently, epoxy resin (EP) was mixed with both F-ND and hydroxylated boron nitride (BN-OH) to produce F-ND/EP and BN-OH/EP composites. Additionally, F-ND: BN-OH ratios of 2:1, 1:1, 1:2 were created for EP combinations (2:1/EP, 1:1/EP, and 1:2/EP). The thermal conductivity of these composites was measured, and the 1:2/EP combination reached a value of 0.94 $W{\cdot}m^{-1}{\cdot}K^{-1}$, showing a 348% increase compared to pure EP and approximately twice the thermal conductivity compared to F-ND and BN-OH alone (Fig. 5A-b). Additionally, as shown in the Fig. 5A-c, the thermal conductivity of the composite showed a tendency to increase with increasing temperature. This highlights how to ND and BN complement each other's high thermal conductivity, significantly enhancing the thermal performance of the composites. To visualize the thermal conductivity effect, the composites were placed on a 100 °C hot plate, and surface temperature changes were measured. After 9 s, the 1:2/EP composites reached 92.5 °C, demonstrating its highest thermal conductivity (Fig. 5A-d) [72]. This results confirms that the combination of F-ND and BN-OH effectively maximizes thermal conductivity. Gulka et al. induced hydroxylation reactions to form -OH functional groups on the surface of ND through non-thermal plasma (NTP) treatment. They examined changes in the zeta potential and FTIR spectra of hydrogen-terminated and oxygen-terminated detonation (DND) and high-pressure high-temperature (HPHT) ND before and after surface modification. The results showed a slight decrease in zeta potential for hydrogen-terminated surfaces and a marked decrease for oxygen-terminated surfaces (Fig. 5B-a). Additionally, as shown in Fig. 5B-b, the FTIR spectra of all samples exhibited changes in free O-H bending and stretching after modification, indicating successful formation of -OH functional groups on the ND surfaces [73]. The introduction of these hydroxyl groups increases hydrophilicity, enhancing cell affinity and improving interactions with tissues, which could play a significant role in wound healing by promoting cellular adhesion and proliferation [74].

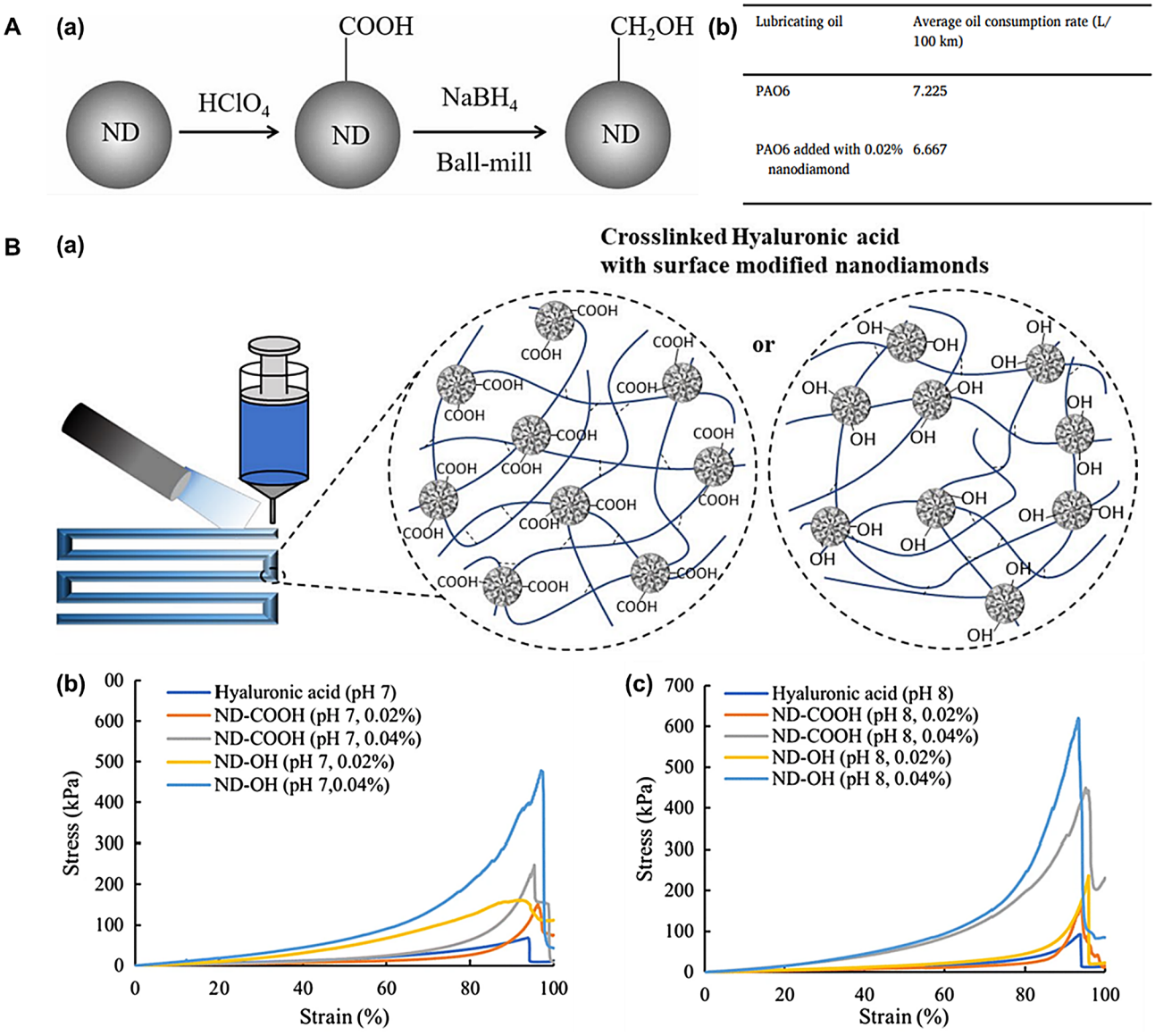

Fig. 4 (**A**): (a) Schematic diagram of the reduction of ND to hydroxyl groups through mechanochemical modification method. (b) The average oil consumption rate with and without ND. Reproduced with permission [70]. (**B**): (a) Schematic diagram of the development of HA/ND nanocomposite hydrogel using carboxylated and hydroxylated ND. Compressive stress-strain curves of HA/ND nanocomposite hydrogels containing ND-COOH and ND-OH at (b) pH 7 and (c) pH 8. Reproduced with permission [71]

Hydrogenation

Hydrogenation can be achieved through thermal annealing or microwave plasma treatment in an hydrogen atmosphere. The mechanism of ND surface hydrogenation primarily involves reactions such as decomposition, decarboxylation and decarbonylation when treated with a mixture of hydrogen and nitrogen. While this approach is straightforward, there is a concern that other species like OH, CH_2, and CH_3 may form on the ND surface under certain conditions, requiring careful consideration [33].

Gim et al. successfully synthesized hydrogenated nanodiamond (H-ND) without graphitization, specifically transforming sp^3 to sp^2 carbon on a carbon substrate (Fig. 6A-a). The hydrogenation of ND, as depicted in the Fig. 6A-b, improved the electrical conductivity of H-ND from $1.95\times10^{-7}\Omega^{-1}cm^{-1}$ to $5.74\times10^{-7}\Omega^{-1}cm^{-1}$. This is because hydrogenation facilitates the mediating ability of ND and its derivatives in electron transfer [75]. As shown in the Fig. 6B-a, Stehlik et al. synthesized detonation ND (DND), bottom-up high-pressure high-temperature ND 8 mm (BU_HPHT ND 8 mm) from chloro-adamantane, and top-down high-pressure high-temperature ND 18 mm (TD_HPHT ND 18 mm) produced by milling HPHT single crystals, and measured their conductivity. As a result, the conductivity of DND decreased to 6.2×10^{-13} S.cm^{-1} immediately after hydrogen annealing.

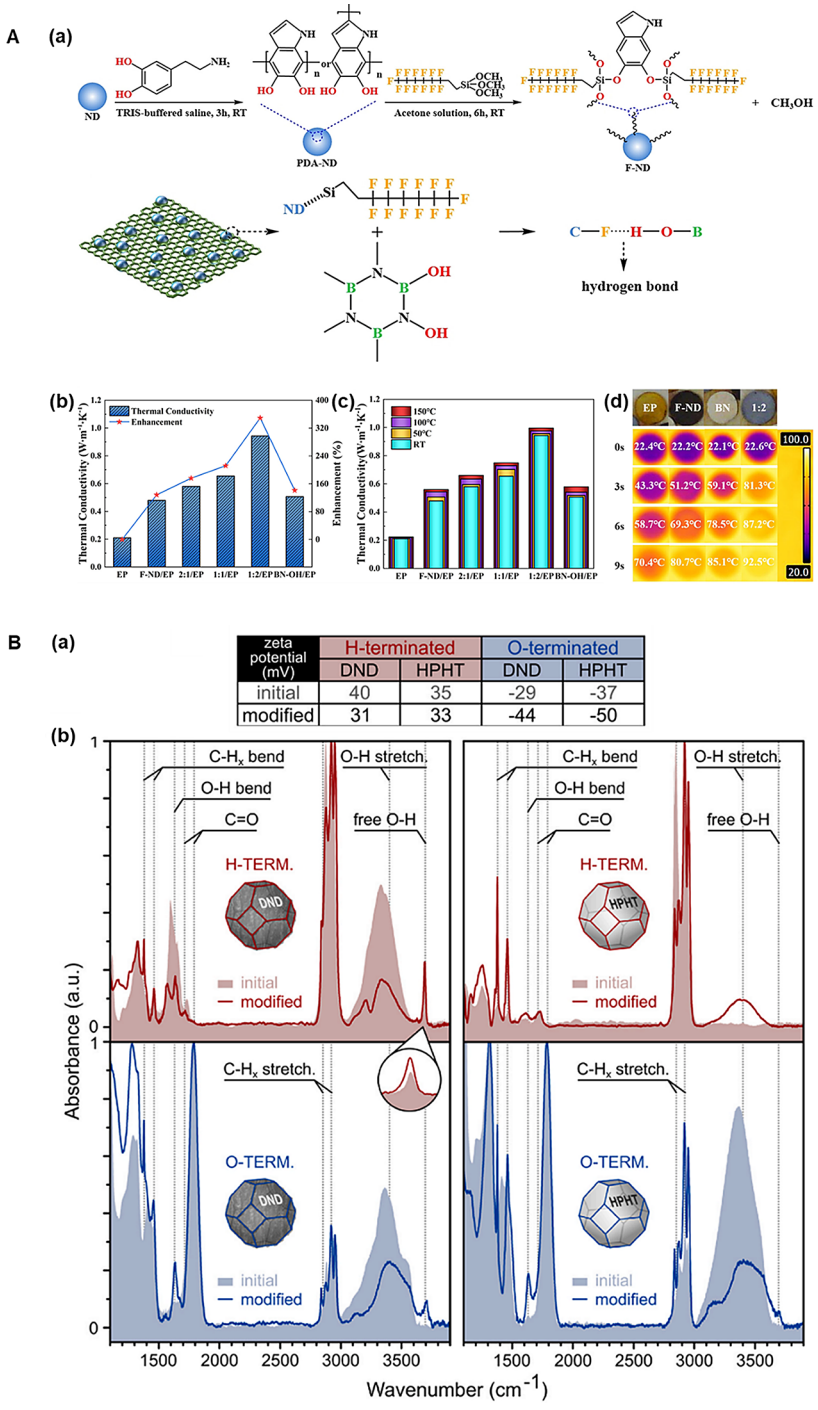

Fig. 5 (**A**): (a) Schematic of surface modification of ND and BN. Thermal conductivity of the composites at (b) Room temperature (c) Room temperature, 50 °C, 100 °C, and 150 °C. (d) Infrared images of changes in the surface temperature of the composite. Reproduced with permission [72]. (**B**): (a) Zeta potential and (b) FTIR spectra changes before and after surface modification of hydrogen-terminated and oxygen-terminated DND and HPHT ND. Reproduced with permission [73]

In contrast, BU-HPHT ND 8 mm, and TD_HPHT ND 18 mm showed an immediate increase in conductivity to 8.7×10^{-6}S.cm^{-1} and 8.5×10^{-6}S.cm^{-1}, respectively, after hydrogen annealing. The reason for these results is as follows: as shown in Fig. 6B-b, DND has a structure with defects in both the surface and the core. The defective surface provides localized energy states where electrons become trapped, resulting in lower conductivity. However, TD_HPHT ND and BU_HPHT ND have lower surface defect density compared to DND, leading to

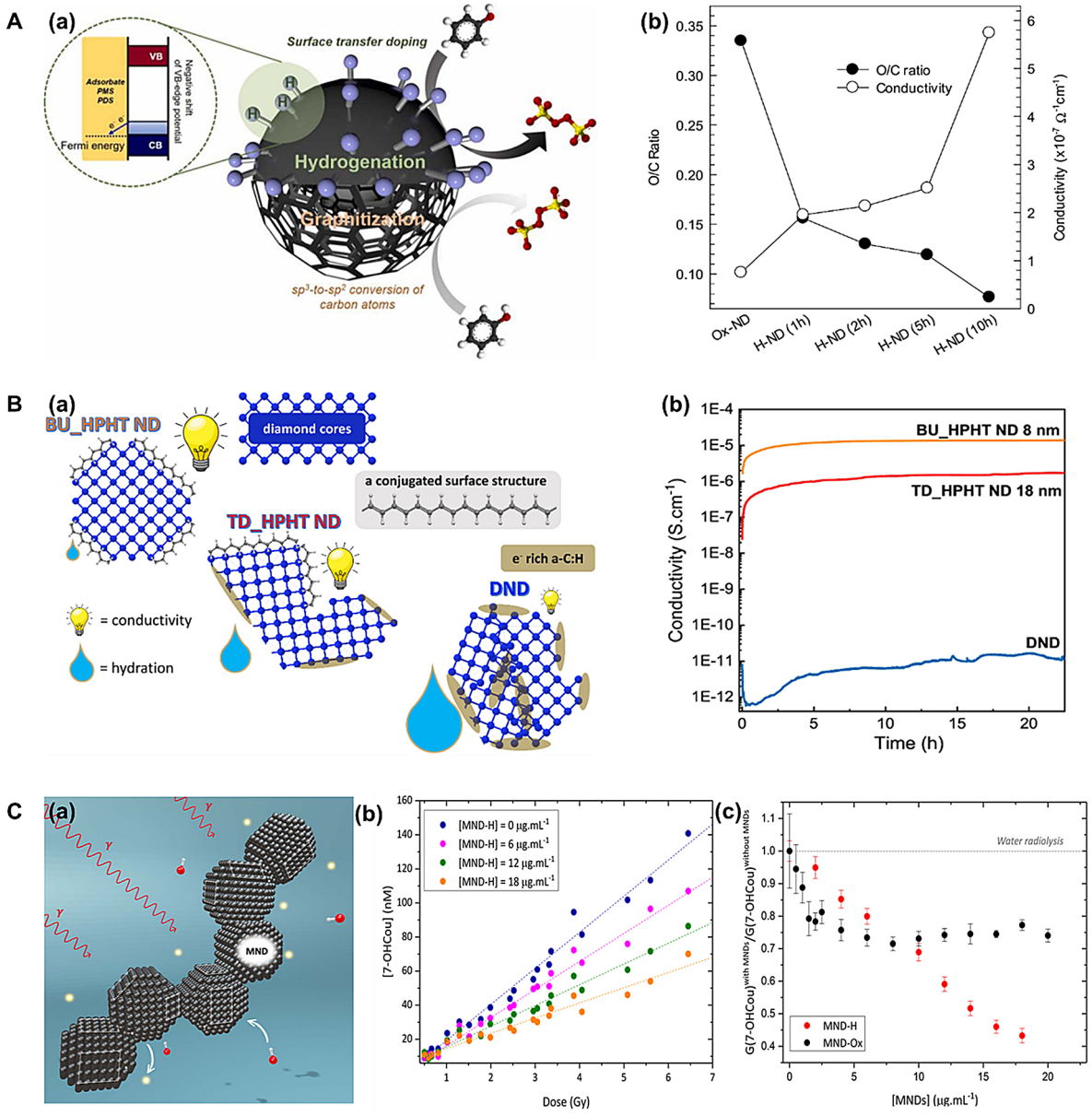

Fig. 6 (**A**): (a) Schematic of the synthesis of H-ND and conversion of sp^3 to sp^2 carbon. (b) O/C ratio and electrical conductivity of Ox/ND, H-NDs. Reproduced with permission [75]. (**B**): (a) Schematic diagram of the structure and conductivity of DND, BU_HPHT ND 8 mm, and TD_HPHT ND 18 mm. (b) Time dependence of the conductivity of the DND, TD_HPHT ND 18 nm and BU_HPHT ND 8 nm. Reproduced with permission [76]. (**C**): (a) Schematic of gamma ray irradiation of MND-ox and MND-H. (b) Graph of the change in 7-OHCou concentration with varying concentrations of MND-H. (c) Graph of the evolution of the apparent formation yields of 7-OHCou for MND-H and MND-Ox. Reproduced with permission [77]

higher conductivity [76]. Ducrozet et al. irradiated aqueous suspensions of oxidized milled ND (MND-Ox) and hydrogenated (MND-H) with gamma rays (Fig. 6C-a). To study the reactivity of MND particles toward hydroxy radicals, they used a coumarin probe to monitor changes in the concentration of 7-hydroxycoumarin (7-OHCou). As shown in Fig. 6C-b, the concentration of 7-OHCou decreased with increasing MND-H concentration. In contrast, MND-Ox showed a decrease in 7-OHCou only up to a concentration of 2.5 µg/mL, beyond which no significant change was observed (Fig. 6C-c). These results suggest that MND-H is more effective than MND-Ox at scavenging radicals, potentially allowing MND-H to serve as a photocatalyst or antioxidant [77].

Amination

Amino groups provide the most useful functional groups for surface modification of ND through various reactions. Amino groups can form amide bonds using established protocols or bind through reductive amination [28, 78].

To introduce NH_2 groups on ND surfaces, methods such as ultraviolet irradiation of hydrogenated diamonds in the presence of chlorine gas or treating chlorinated ND with ammonia at high temperatures can be used [79, 80]. Additionally, amination on ND can be achieved through further covalent or non-covalent reactions with hydrogenated, carboxylated, or hydroxylated ND [81].

Alwani et al. oxidized lysine amino acids onto the carboxylated surface of ND in an oxidative acid throughout the synthesis process, resulting in the covalent bonding of lysine. This led to the synthesis of lysine-functionalized ND (Lys-ND). Zeta potential and particle size measurements showed that Lys-ND exhibited minimal precipitation and good stability. Additionally, they investigated the intracellular transport pathways. The results revealed that while pristine ND (pND) was found in vesicular aggregates, Lys-ND was evenly distributed in the cytoplasm and existed as uniformly sized particles. This suggests that the aminated Lys-ND is more effective for gene delivery and other intracellular applications [82]. Ryu et al. modified ND with carboxyl groups on the surface, converting them into aminated ND using ethylenediamine. Then they conjugated folic acid (FA) to the aminated ND using carbodiimide chemistry, synthesizing FA-ND nanoclusters (Fig. 7A-a). After intravenous injection of the FA-ND, near-infrared (NIR) irradiation was applied to observe an increase in the temperature of the tumor in vivo. As shown in Fig. 7A-b, during the 5 min NIR irradiation, the temperature change is due to rapid heat generation on the ND surface from light absorption under NIR irradiation, followed by a quick drop in temperature as the NIR energy source is removed. These findings that FA-ND have potential for photothermal tumor therapy [83]. In another study, Ashek-I-Ahmed et al. annealed ultra disperse diamond (UDD), synthesized through the detonation method, at 800 °C in a vacuum to modify the ND surface with amine groups (Fig. 7B-a). At 500 °C, two distinct peaks attributed to C-H bonds appeared in the 2875–2945 cm^{-1} range, as shown in Fig. 7B-b(ii). These peaks indicate the presence of carbon from the tetrahedral diamond lattice of ND. At 800 °C, the peak corresponding to the nitrile group (-C≡N) disappeared completely, as illustrated in Fig. 7B-c(iv). Conversely, a clear band in the 3200–3450 cm^{-1} range, indicative of the symmetric and asymmetric stretching vibrations of the primary amine (NH_2), was observed, as shown in Fig. 7B-d(iv). This indicates that the nitrile group was hydrogenated and reduced to amine, confirming the successful surface of ND to amine [54]. Li et al. synthesized diamane nanoflakes, a two-dimensional ND using the high-temperature high-pressure (HTHP) method, followed by ball milling to physically exfoliate them. Then, they functionalized the nanoflakes with ammonia and subjected them to thermolysis at 400 °C to produce amino-functionalized NH_2-diamane nanoflakes (Fig. 7C-a). Finally, these nanoflakes were coated onto polypropylene (PP) to fabricate the PP/NH_2-diamane separator. Mechanical strength analysis revealed that the average Young's modulus of PP/NH_2-diamane was 4.16 GPa, which was significantly higher than that of pure PP (0.035 GPa) (Fig. 7C-b). This indicates that the integration of amino-functionalized ND onto the PP surface substantially enhances its mechanical strength. Furthermore, under the same laser heating conditions (400 mW), the maximum central temperature of PP/NH_2-diamane was 60.1 °C, which was lower than that of pure PP (83.7 °C) (Fig. 7C-c) These results suggest that the incorporation of amino-functionalized ND provides excellent thermal conductivity, promoting uniform heat diffusion, which enhances cellular activity and accelerates skin tissue regeneration [84].

Halogenation

Halogenation of ND is a method to activate the surface by generating electrophilic centers that can further react with nucleophilic reagents. Fluorination can be achieved by reacting the ND surface with a mixture of F_2/H_2 gases at high temperatures. Alternatively, sulfur hexafluoride (SF_6) can be used in atmospheric pressure plasma treatments to introduce C–F bonds. Chlorinated ND can be prepared through thermal treatment with Cl_2 or CCl_4[4], or by exposing hydrogenated ND to chlorine gas under UV irradiation. Halogenation, such as chlorination and fluorination of ND, results in highly photostable materials, making them ideal for applications such as cell tracking and imaging due to their enhanced stability [85, 86].

Ekimov et al. successfully synthesized ultrasmall ND under high-pressure, high-temperature (HPHT) conditions, using halogenated adamantane ($C_{10}H_{14}Br_2$) at a fixed pressure of 8GPa. The halogenated adamantane acted as a crucial precursor in ND synthesis, suggesting that it is effective in altering the surface chemical properties of the ND [87]. Additionally, they demonstrated the successful synthesis of ultrafine ND using fluorinated 1-fluoroadamantane under similar HPHT conditions, showing that halogen atoms can influence the structure and characteristics of the resulting ND [88]. Zhou et al. synthesized HND-Cl and BND-Cl by irradiating hydrogenated surface ND (HNDs) and graphitized surface ND (BNDs) in air-free environment of CCl_4, $CHCl_3$, and CH_2Cl_2, using a linear electron accelerator at doses up to 1100 kGy (Fig. 8A-a). They confirmed the attachment of chlorine to the ND surfaces. As shown in Fig. 8A-b, no chlorine-specific signal at m/z = 36 was observed for HND and BND before chlorination. However, after chlorination, a strong signal was detected for HND-Cl and BND-Cl. Additionally, the release of -Cl occurred over a broad temperature range from 50 °C to 450 °C, indicating

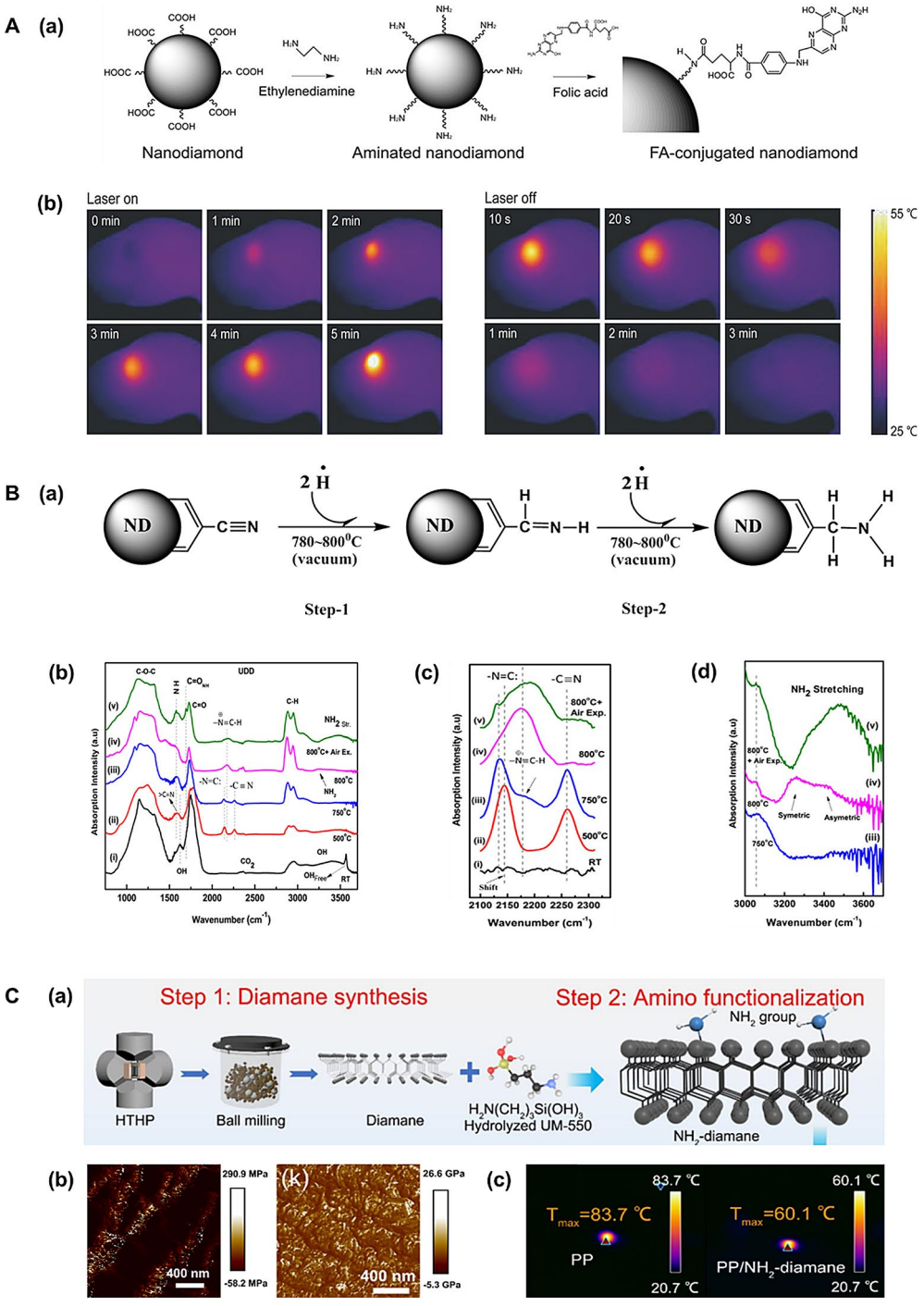

Fig. 7 (**A**): (a) Schematic diagram of FA-ND nanocluster synthesis process. (b) In vivo thermal imaging images of mice with tumors irradiated locally with NIR laser 5 min, 72 h after intravenous injection of FA-ND nanocluster. Reproduced with permission [83]. (**B**): (a) Schematic diagram of the process for modifying the UDD surface with amine groups under vacuum conditions at 780–800 °C. FTIR spectra of (b) untreated UDD, surface modified UDD in the range of (c) 1400–1840 cm^{-1}, and (d) 3000–3650 cm^{-1}. Reproduced with permission [54]. (**C**): (a) Schematic diagram of NH_2-diamane synthesis process. (b) Young's modulus of pure PP and PP/NH_2-diamane. (c) Maximum central temperature upon the introduction of the laser beam to the surface of PP and PP/NH_2-diamane. Reproduced with permission [84]

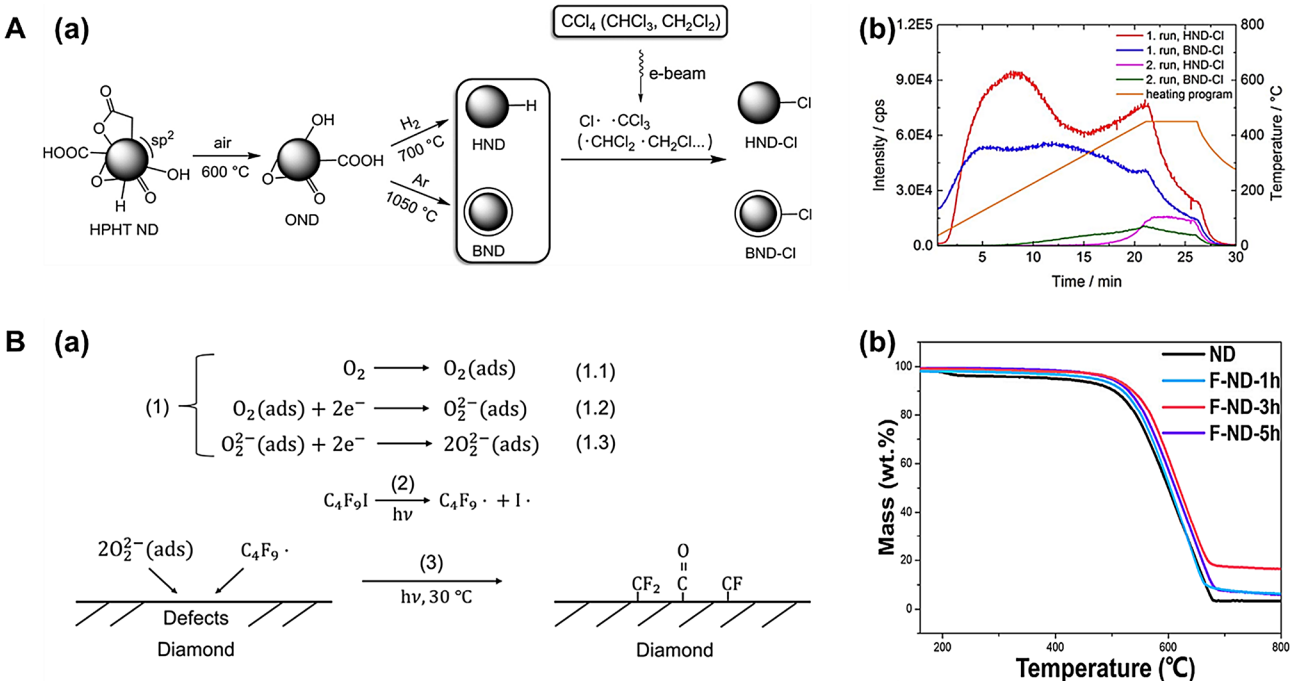

Fig. 8 (**A**): (a) Synthesis mechanism of HND- Cl and BND-Cl. (b) Temperature-time profile graph of the fragment m/z = 36 for HND and BND before and after chlorination. Reproduced with permission [89]. (**B**): (a) Synthesis mechanism of F-ND. (b) TGA experimental curve of ND and F-NDs. Reproduced with permission [90]

that chlorine bonds of various types were formed on the ND surface [89]. Luo et al. immersed ND nanoparticles in a C_4F_9I solution and subjected them to photoinitiation with a xenon lamp for several hours to synthesize fluorinated ND (F-ND), with the related mechanism proposed in Fig. 8B-a. The results confirmed that the fluorinated ND treated for 3 h (F-ND-3 h), exhibited the highest thermal stability and oxidation resistance (Fig. 8B-b) [90]. This suggests that F-ND can maintain its structure and properties when exposed to body temperature or external heat sources, and its excellent resistance to oxidative stress in the biological environment may positively influence wound healing.

Thermal conductivity

Diamond itself possesses an ultra-high thermal conductivity of approximately 2000 W/(m·k) [91]. Therefore, ND, based on this property, also exhibits excellent thermal conductivity. The thermal conductivity of ND varies depending on its structure [92]. Due to this property, ND provides thermal stability to fibrous materials, enabling them to withstand high-temperature conditions without a loss strength. Furthermore, as shown in Table 2, ND exhibits superior thermal conductivity compared to other carbon-based materials.

Thus, it acts as a key factor in achieving rapid temperature elevation under near-infrared (NIR) irradiation within a short period (Table 3). This is attributed to the ability of ND to efficiently convert absorbed light energy into heat and rapidly dissipate the generated heat throughout the material. The high thermal conductivity prevents the localized accumulation of thermal energy and ensures uniform distribution across the material, enabling the formation of high-temperature zones in a short time. These characteristics demonstrate that ND exhibits superior performance in thermal energy transfer and dissipation compared to other carbon-based materials [107].

In practice, ND-based nanofibers with high thermal conductivity offer several advantages as wound dressings. The high thermal conductivity allows for photothermal therapy or heat-based wound healing, which can effectively contribute to infection prevention and bacterial eradication. Additionally, the high thermal conductivity enables rapid and uniform heat distribution to the wound site, facilitating localized treatment without causing damage to surrounding tissues, and it can also promote the activation of antimicrobial agents [122, 123]. However, if the thermal conductivity is excessively high, there is a risk of excessive heat being transferred to the wound area, potentially causing damage to the surrounding healthy tissues. Moreover, at elevated temperatures, physical and chemical stability issues may arise in the nanofibers, which could negatively affect the functionality or biocompatibility of the ND-based material [124, 125]. Therefore, the application of ND-based nanofibers with high thermal conductivity as wound dressings requires careful design that considers heat management

Table 2 Thermal conductivity of various carbon-based materials

Material	Formulation	Thermal conductivity [W/(m·k)]	Ref
Graphene	Polypropylene/graphite/graphene	8.65	[93]
	Micron-diamond@ graphene nanoplatelets/ nanofibrillated cellulose	5.66	[94]
	Poly(l-lactide)/ graft-graphene nanoplatelets-poly(d-lactic acid)	1.12	[95]
Graphite	Paraffin@ graphite felt	0.68	[96]
	Epoxy/carbon fiber/carbon/ graphite	6.2	[97]
	Carbon nanotubes pillared exfoliated graphite/polyimide	1.92	[98]
Carbon nanotube	Boron nitride nanosheets/ carbon nanotube/epoxy resin	0.84	[99]
	Carbon nanotube-graphene/ polydimethylsiloxane	4.641	[100]
	Carbon nanotube/ Au in evaporated porous Al-doped ZnO	2.21	[101]
Carbon dot	3D Graphene quantum dots/ zinc oxide	0.785	[102]
	MXene/carbon dot	0.945	[103]
Nanodiamond	Uniaxial-polyvinyl alcohol/ nanodiamond	81.3	[104]
	Poly(vinyl alcohol)/ hydroxyl-rich nanodiamonds	18.98	[105]
	Cellulose nanofiber/ single-crystal nanodiamond	76.23	[106]

techniques and material stability. Based on the characteristics described above, the following example is provided below. Wang et al. developed poly (diallyldimethylammonium chloride)-functionalized nanodiamond/aramid (ND@PDDA/ANF) nanofibers. As shown in the Fig. 9A-a and b, ND@PDDA/ANF nanofibers demonstrated high in-plane and through-plane thermal conductivities of 30.99 and 6.34 W/(m·k), respectively. The through-plane thermal conductivity was the highest reported value among all insulating polymer-based composite supports (Fig. 9A-c) [126]. In another study, Song et al. developed hydrophobic nanofiber cellulose-graphene (HNG) by spraying polydopamine-modified nanodiamond (F-PDA-ND) onto nanofiber cellulose (NFC) and pyrene-aminated graphene ($PyHN_2$@G). The thermal conductivity of HNG-10 (containing 10wt% $PyNH_2$@G) was measured to be 27.06 W/(m·k), representing a 21.36-fold increase [127]. Furthermore, Jiao et al. developed a flexible cellulose nanofiber (CNF)/nanodiamond (ND)/MXene (CNM) composite platform. As shown in Fig. 9B-a, pure CNF displayed relatively low thermal conductivities of 2.63 W/(m·k) horizontally and 0.16 W/(m·k) vertically. However, adding just 2phr of ND increased the thermal conductivity to 9.81 W/(m·k) and 0.24 W/(m·k), showing enhancements of 273% and 50%, respectively. Moreover, the addition of ND had a significant impact on the thermal conductivity of CN0M30. According to the Fig. 9B-b, adding 5phr of ND led to a sharp increase in thermal conductivity from 7.98 W/(m·k) to 16.49 W/(m·k). Consequently, as shown in Fig. 9B-c, it can be clearly observed that the in-plane and out-of-plane thermal conductivities of the composite platform tend to increase sharply with the addition of ND. This enhanced thermal conductivity is attributed to ND acting as thermal bridges between the MXene sheets, arranged in a layered structure, which improves heat flow between the MXene layers (Fig. 9B-d) [128]. Song et al. fabricated an NFC/ND hybrid support using nanofibrillated cellulose (NFC) and ND. Thermal conductivity measurements, both in-plane and through-plane, revealed that the thermal conductivity significantly improved with increasing ND content (Fig. 9C-a). Notably, with only 0.5wt% ND loading, the in-plane thermal conductivity increased substantially from 1.122 W/(m·k) to 9.820 W/(m·k), representing a remarkable increase of approximately 775.2%. As shown in Fig. 9C-b, the thermal conductivity measured in such NFC/ND composites is notably high compared to previous studies. The intermolecular hydrogen bonding between the -OH and -COOH groups of ND particles and the -OH groups of NFC enhances the adhesion between ND and NFC, facilitating the formation of more efficient thermal conduction pathways (Fig. 9C-c). Additionally, the unique anisotropic properties of the 1D NFC structure promote the formation of a hierarchical structure, which supports the creation of thermal conduction pathways facilitated by the ND particles dispersed within the NFC network (Fig. 9C-d) [129].

Wettability

Generally, a contact angle of less than 90° indicates that a surface is considered hydrophilic, particularly when it is oxygen-terminated. In contrast, surfaces that are hydrogen-terminated, with a contact angle exceeding 90°, are classified as hydrophobic [130, 131]. Nanofibers containing ND exhibit these hydrophilic characteristics, which contribute to their moisture absorption and management properties [132]. Due to these characteristics, it can effectively retain moisture, optimizing the environment of the wound site to prevent infection and enhance the healing speed. Additionally, it promotes cell diffusion and adhesion, playing a highly effective role in wound healing [133]. For example, Olăreț et al. fabricated nanofibers using fish gelatin (FG) at 50% (w/v) and 70% (w/v) concentrations (FG50, FG70) as control groups, and nanofibers containing ND (FG50_ND, FG70_ND) as experimental groups (Fig. 10A-a). Contact

Table 3 Temperature rise characteristics of various carbon-based materials under NIR irradiation

Material	Formulation	Wave length (nm)	Time [min]	Temp [°C]	Application	Ref
Graphene	Reduced graphene oxide@ poly(methyl methacrylate) coated with reduced graphene oxide/ polyethylenimine bilayers	808	8	27.6 ± 1.8	Photothermal therapy	[108]
	Graphene oxide/ poly (L-lactide-co-ε-caprolactone	808	1.5	43.5	Antibacterial	[109]
	Few-layer graphene oxide	812	45	56	Antibacterial	[110]
Graphite	Graphite derived carbon dots	808	10	27.9	Photothermal therapy	[111]
	Coconut fibers/ recycled polystyrene/ graphite	808	90	56.9	Photothermal conversion	[112]
Carbon nanotube	Poly (ε-caprolactone)/ gelatin/ carbon nanotubes-photoluminescent mesoporous silica nanoparticles	808	10	20	Drug delivery platform release	[113]
	Bi_2Se_3 nanosheets/ carbon nanotubes	808	8.5	54.1	Photothermal, biocompatibility	[114]
	Konjac glucomannan-sodium alginate@ carbon nanotubes/Fe^{3+}	808	5	56	Antibacterial	[115]
Carbon dot	Iron-doped carbon dots	808	10	45.5	Antibacterial, wound healing	[116]
	Cellulose nanofiber/ carbon quantum dot	350	-	~30	Photothermal	[117]
	Graphene quantum dots- semiconducting polymer nanocomposites	808	5	47	Photothermal therapy, biocompatibility	[118]
Nanodiamond	Iron oxide nanoparticles@ nanodiamond	808	3	67.6	Photothermal therapy	[119]
	Acrylic-grafted chitosan-oxidized hyaluronic acid-nanodiamond	808	5	70	Antibacterial, wound healing	[120]
	Polyurethane-grafted nanodiamond/multi-walled carbon nanotubes	808	1	105.1	Photothermal	[121]

angle measurements showed that the addition of ND resulted in a lower contact angle in both FG50_NDs and FG70_NDs compared to the control, indicating enhanced hydrophilicity (Fig. 10A-b) [134]. As shown in the Fig. 10B-a, Narla et al. functionalized ND using ball milling with polypropylene glycol (PPG) and a silane coupling agent (ND-Si-PPG-CH_3). Subsequently, they fabricated PVDF-HFP@5%ND nanofibers using ND with a mass fraction of 5% (by weight relative to the polymer) and poly(vinylidene fluoride-co- hexafluoropropylene) (PVDF-HFP). Compared to polypropylene (PP), the PVDF-HFP@5%ND nanofibers exhibited a very low contact angle of 20°, indicating a strong affinity for the electrolyte (Fig. 10B-b) [135]. Houshyar et al. fabricated nanofibers by adding ND to wool fabric. The 0%w/w ND sample (W_0) was designated as the control group, while the nanofibers with 0.1%w/w, 0.2%w/w, and 0.3%w/w ND were abbreviated as W_1, W_2, and W_3, respectively. As shown in the Fig. 10C-a, the contact angle of the untreated W_0 ranged from 119° to 125°. However, after treatment with ND, W_1 exhibited a low contact angle of less than 20°, while W_2 and W_3 showed values close to 0° (Fig. 10C-b, c, and d). This indicates that the hydrophilicity increases with a higher concentration of ND on the nanofiber surface, as there are more polar groups such as -OH and COO- present (Fig. 10C-e) [136].

Nanofibers containing ND also possess hydrophobic properties, which prevent excessive moisture absorption at the wound site, providing a stable environment. This promotes cell migration and proliferation, while facilitating drug delivery, allowing for the continuous release of antimicrobial or anti-inflammatory agents necessary for wound healing. These properties enhance the efficiency of wound healing and contribute to infection prevention [137–140]. In a study performed by Zhang et al., they fabricated ND-reinforced polyurethane (NDs/PU) nanofibers (Fig. 10D-a). As shown in Fig. 10D-b, the contact angle measurements revealed that pure PU nanofibers exhibited a contact angle of 115.7°. However, with the addition of ND, the contact angles increased to 135.4° and 139.7° for 5.5wt% NDs/PU and 7.5wt% NDs/PU, respectively. This significant increase in contact angle demonstrates the superior hydrophobicity of the NDs/PU nanofibers, which is even better than previously

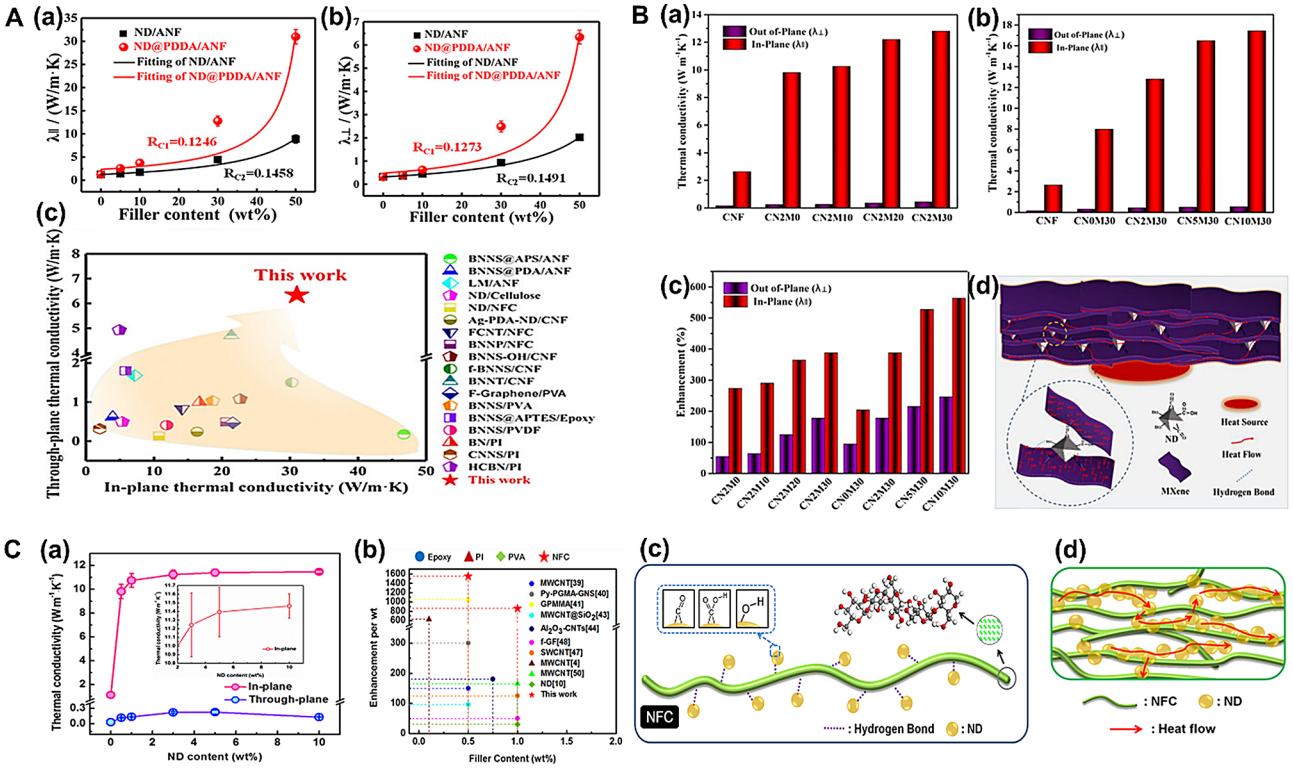

Fig. 9 (**A**): The (a) in-plane and (b) through-plane thermal conductivity graphs of ND@PDDA/ANF nanofibers. (c) Comparison of through-plane thermal conductivity between all insulating polymer-based composites and this study. Reproduced with permission [126]. (**B**): Out of-plane and in-plane thermal conductivity graphs with different (a) MXene and (b) ND content. (c) Improvement in thermal conductivity of CNM platform compared to CNF platform (d) Schematic diagram of thermal conductivity of composite platform. Reproduced with permission [128]. (**C**): (a) In-plane and through-plane thermal conductivity graphs of NFC/ND as a function of ND concentration. (b) Comparison graph of thermal conductivity per weight of this study with other polymer-based composites. (c) Schematic of intermolecular hydrogen bonding between ND and NFC. (d) Schematic of thermal conduction pathways in NFC/ND. Reproduced with permission [129]

reported results (Fig. 10D-c) [141]. Hence, ND-based nanofibers, depending on the modifications, possess both hydrophilic and hydrophobic properties, which can work in harmony depending on the wound healing environment, ultimately contributing to the optimization of the healing process.

Porosity

The porosity of nanodiamond-incorporated nanofibers plays a critical role in enhancing wound healing by optimizing the wound microenvironment and enabling advanced therapeutic functions. The highly porous network of nanofibers (78–93% porosity in various compositions [142]) mimics the extracellular matrix, facilitating cell adhesion, migration, and proliferation while allowing oxygen diffusion and moisture retention [138, 139, 142]. This architecture provides an ideal scaffold for embedding NDs, which can be uniformly distributed within the fibrous matrix to achieve controlled release of therapeutic agents like siRNA or antibiotics [120, 143]. The interconnected pores simultaneously absorb wound exudate and maintain hydration, preventing bacterial colonization while promoting angiogenesis and re-epithelialization [142]. When combined with nanodiamonds, the enhanced surface area from porosity improves drug-loading capacity and sustains antibacterial activity, as demonstrated by hydrogel systems achieving 90–93% bacterial eradication [120]. Furthermore, tailored porosity enables sequential release kinetics–rapidly delivering hemostatic agents while gradually releasing growth factors to coordinate inflammatory and proliferative healing phases [143]. Studies show diabetic wound models treated with these porous nanocomposites exhibit accelerated closure rates (93% improvement in epithelialization) and reduced MMP-9 levels through optimized siRNA delivery [143].

Biocompatibility

Biological materials can withstand the influence of various biological systems within an organism and maintain relatively stable characteristics without rejected or damaged. ND exhibit excellent biocompatibility in biological applications. The biocompatibility of ND stems from the chemical inertness of diamond nanocrystals and the absence of toxic chemical release from the nanocrystals [144, 145]. Table 4 below presents the biocompatibility

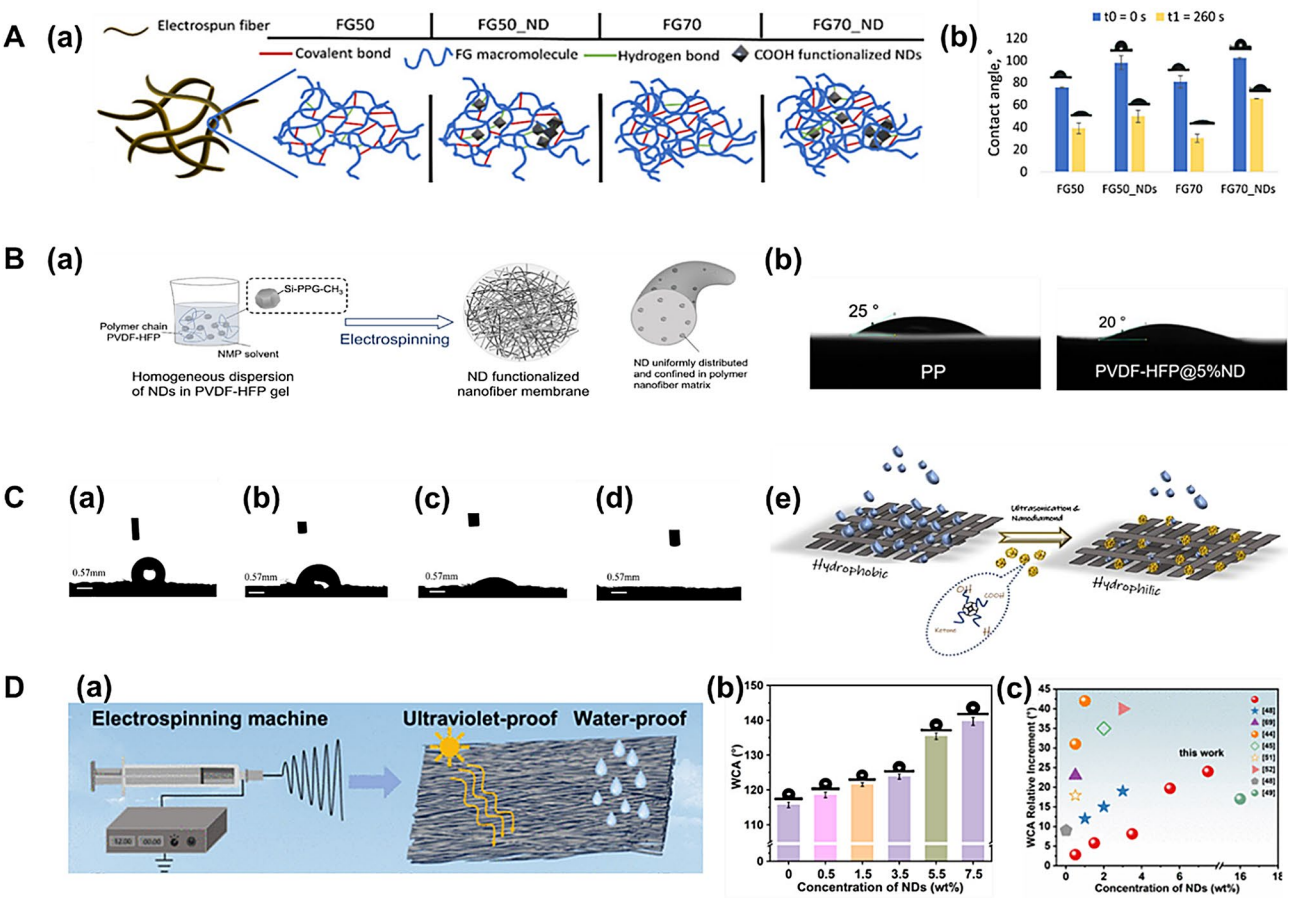

Fig. 10 (**A**): (a) Schematic representation of FG50, FG50_ND, FG70, and FG70_ND nanofibers. (b) Contact angle graphs of FG50, FG50_ND, FG70, and FG70_ND immediately after droplet deposition and 206s later. Reproduced with permission [134]. (**B**): (a) Schematic of fabrication of ND-functionalized nanofibers. (b) Comparison of the contact angle of a water droplet between PP and PVDF-HFP@5%ND. Reproduced with permission [135]. (**C**): Contact angle of a water droplet on (a) W_0 (b) W_1 (c) W_2 and (d) W_3. (e) Schematic diagram of mechanisms for hydrophilic properties that increase with ND addition. Reproduced with permission [136]. (**D**): (a) Schematic diagram for the fabrication of NDs/PU nanofibers. (b) Water contact angle graph according to ND content. (c) Comparison graph of water contact angle between this study with previous studies. Reproduced with permission [141]

Table 4 Effects of ND nanofiber composites on various cell lines and their applications

Material	ND content	Cell type	Properties	Ref
Poly-ε-caprolactone	2%	Schwann cell	Promotion of cell proliferation and adhesion, regulation of macrophage polarization	[146]
	0.5, 1, 2, 3wt%	Mouse calvaria-derived pre-osteoblast	1wt.% of ND/PCL: Cell proliferation rate approximately 1.5 times (compared to PCL), improve alkaline phosphatase activity	[147]
	0.1%w/w	Human lens epithelial	No toxicity	[148]
Poly(lactic-co-glycolic acid)	5%	Natural stem cell	Survival rate of cells: 85%	[149]
	0.7wt%	Human mesenchymal stem cells	Improved cell diffusion due to increased hydrophilicity	[150]
Gelatin from cold water fish	0.5 and 1%	Human adipose-derived Stem	Cells remain viable after 48 h, cell adhesion, no cytotoxicity	[151]
Polypropylene	1%w/w	Chinese hamster ovarian cells	Very high cell adhesion compared to control, with longer cells and more filopodia	[152]
Silicon oxide	-	Human osteoblast-like Saos-2cells	Support cell adhesion, spreading, and proliferation, high collagen and ALP synthesis, and calcium precipitation on day 14 of cell culture	[153]

characteristics and applications of nanofiber composites utilizing ND on various cell lines.

Biodegradability

The biodegradability of nanofibers is crucial in wound healing as it allows gradual tissue replacement while maintaining structural support, preventing secondary damage from frequent dressing changes [154, 155]. This property ensures optimal compatibility with healing phases, enabling controlled release of therapeutic agents and eliminating the need for manual removal, which reduces inflammation and promotes complete regeneration [156]. The biodegradability of NDs and ND-incorporated nanofibers depends on the composite materials and environmental conditions. While NDs themselves are chemically inert and not inherently biodegradable, their incorporation into biodegradable polymers like PLA or chitosan/bacterial cellulose blends enables controlled degradation of the composite matrix [157–159]. Studies show PLA films with embedded NDs degrade gradually under alkaline conditions (pH 10), with erosion rates correlating to increased ND mobility and reduced polymer viscosity, though degradation is minimal at neutral pH [157, 159]. In chitosan-based nanofibers, NDs (1–3 wt%) enhance mechanical strength while maintaining biocompatibility, though higher concentrations lead to nanoparticle agglomeration and reduced durability [42]. The biodegradation process of these composites typically involves polymer chain breakdown through hydrolysis or enzymatic action, while NDs remain intact and may persist in the environment [86, 159]. This persistence raises concerns about long-term accumulation, as ND's small size and surface functional groups could theoretically enable gradual breakdown under specific physiological conditions, though conclusive evidence remains limited [141]. Current research indicates that while the polymer matrices can degrade within weeks to months depending on composition, the ND components require further investigation regarding their environmental fate and potential metabolic clearance pathways [86, 159].

Moreover, the incorporation of NDs into polymers influences biodegradation rates through complex interactions dependent on environmental conditions and material composition. Under alkaline conditions (pH 13), nanodiamond-embedded polylactic acid (PLA) films exhibit accelerated degradation, as nanodiamond mobility increases with polymer erosion, correlating with reduced viscosity and enhanced gadolinium ion diffusion near the NDs [157]. This mobility enables real-time tracking of degradation via nanodiamond magnetometry, which measures spin relaxation (T1) changes as the polymer matrix breaks down. However, at neutral pH (7) or mildly alkaline pH (10), PLA degradation is minimal, with NDs showing negligible mobility changes, suggesting pH-dependent modulation of degradation kinetics. NDs may indirectly affect biodegradation by altering polymer structure—higher concentrations (1–3 wt%) in chitosan-based composites improve mechanical stability but can agglomerate, potentially slowing enzymatic or hydrolytic breakdown [160]. Surface-functionalized NDs (e.g., carboxylated or aminated variants) may further influence degradation through electrostatic interactions with microbial membranes or polymer chains, though cytotoxicity risks require careful optimization [161]. While the polymer matrix degrades via hydrolysis or microbial action, NDs themselves remain chemically inert, persisting post-degradation and raising concerns about long-term environmental accumulation [157]. Thus, their primary role lies in enabling degradation monitoring rather than actively accelerating the process under physiological conditions.

Antioxidant activity

Antioxidant activity involves neutralizing excess reactive oxygen species (ROS) that disrupt cellular membranes, DNA, and proteins, while preserving beneficial low-level ROS required for antimicrobial defense and cell signaling during wound repair [162, 163]. In wound healing, antioxidants mitigate oxidative stress to accelerate fibroblast proliferation, collagen deposition, and angiogenesis, while balancing inflammation. For antibacterial applications, antioxidants prevent microbial proliferation exacerbated by ROS-induced tissue damage, synergizing with antimicrobial agents [164]. NDs exhibit intrinsic antioxidant properties through surface functional groups (-OH, -COOH) and C = C bonds that scavenge ROS. Hydroxylated NDs reduced lipid peroxidation in microalgae by 50% under oxidative stress, preserving photosynthetic efficiency [21]. When incorporated into nanofibers, NDs enhance composite functionality. For example, polyvinylpyrrolidone/cerium/curcumin nanofibers achieved 100% wound closure in 20 days via synergistic antioxidant effects (95% radical scavenging) [163]. NDs also amplify antibacterial effects through surface charge interactions and oxidative stress induction. Acid anhydride groups on ND surfaces disrupt bacterial membranes, while graphitic layers potentiate antibiotic delivery [86]. For example, ND-fullerene composites reduced biofilm viability by 80% through dual ROS scavenging and physical cell wall damage [164]. These multifunctional systems address infected wounds by concurrently resolving oxidative imbalance and microbial colonization.

Wound healing application of ND-based nanofiber

Antibacterial effect

ND-based nanofibers exhibited excellent antibacterial properties. ND has a highly modifiable surface, enabling it to generate reactive oxygen species (ROS), which

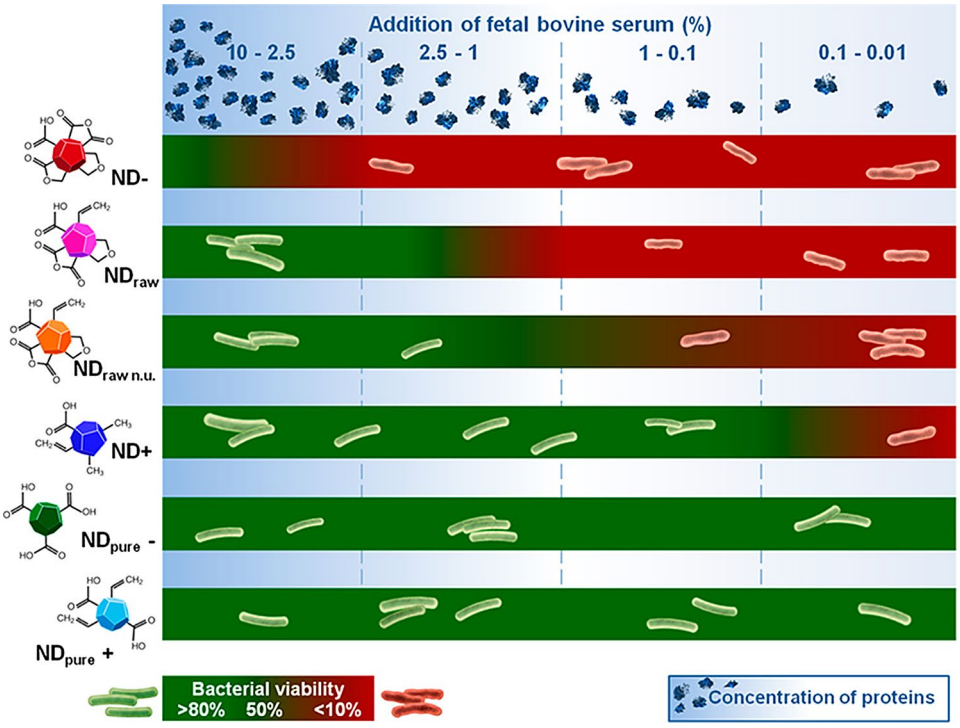

Fig. 11 Schematic of the antibacterial effect characteristics of surface-modified ND (ND-and ND_{Pure} -: air atmosphere annealing, ND + and ND_{pure} +: Hydrogen (H_2) atmosphere annealing, ND_{raw} and $ND_{raw\ n.u}$: No annealing). Reproduced with permission [167]

enhance its antibacterial activity (Fig. 11). Additionally, the high surface area and conductivity of ND allow it to disrupt bacterial cell membranes and inhibit bacterial growth. Under NIR stimulation, ND generates heat and ROS, which damage bacterial proteins and nucleic acid, effectively rupturing bacterial membranes and eradicating biofilms. These properties make ND-based nanofibers valuable for preventing infections and inhibiting bacterial growth during the wound healing process [165, 166].

Wu et al. fabricated PLA/ND fibers using poly-lactic acid (PLA) and ND, and coated them with β-chitin to developed C/PLA/ND scaffolds. They evaluated the antibacterial activity by measuring the growth and survival of *Staphylococcus aureus* (*S. aureus*) and *Escherichia coli* (*E. coli*). As shown in Fig. 12A-a, the red arrows highlight dead bacteria, while the survival rate of bacteria remained high in the control groups and pure PLA. In contrast, the C/PLA/ND scaffolds exhibited approximately 50% bacterial mortality for both bacteria (Fig. 12A-b). Additionally, as demonstrated in Fig. 12A-c and d, the proliferation of both bacteria was inhibited [168]. These findings suggest that the incorporation of ND and β-chitin into PLA scaffolds enhances their antibacterial properties and biocompatibility, making them a promising platform for effective wound healing applications. In another study, Khalid et al. fabricated Silk, $ND_{0.25}$-silk, and $ND_{0.5}$-silk nanofiber platforms by incorporating ND at concentrations of 0 mg/mL, 0.25 mg/mL, and 0.5 mg/mL, respectively. They evaluated the antibacterial properties against *Pseudomonas aeruginosa* (*P. aeruginosa*) and *E. coli*, two major pathogens responsible for skin wound infections. SEM image analysis revealed that both bacteria failed to extensively adhere to ND-silk nanofibers, showing flattened and damaged forms (Fig. 12B-a). The number of bacteria attached to the nanofibers was less than 1000/mm^2, with *E. coli* showing fewer than 200/mm^2, which is below detection limits. Furthermore, confocal laser scanning microscopy (CLSM) imaging of ND-silk demonstrated an average antibacterial efficiency of approximately 99% and 95% against *P. aeruginosa* and *E. coli*, respectively, confirming high antibacterial activity against both bacteria (Fig. 12B-b). As seen in Fig. 12B-c, SEM analysis further revealed the damaged cell (orange color) morphology of bacteria within ND-silk nanofibers [169]. These results demonstrate strong antibacterial effects which indicates that ND-based silk structures do not exhibit inherent resistance to bacteria, and such structures provide superior antibacterial properties, helping to minimize infection risks in wound healing.

Karami et al. prepared ND-EDA by surface modification ND through carboxylation, chlorination, and amination to attach ethylenediamine (EDA). ND-EDA was then applied to the polyamide surface of Thin Film Composite (TFC) scaffolds at concentrations of 250, 500, 1000ppm, resulting in TFC-250, TFC-500, TFC-1000, respectively. For comparison, TFC-0 (without ND-EDA) and

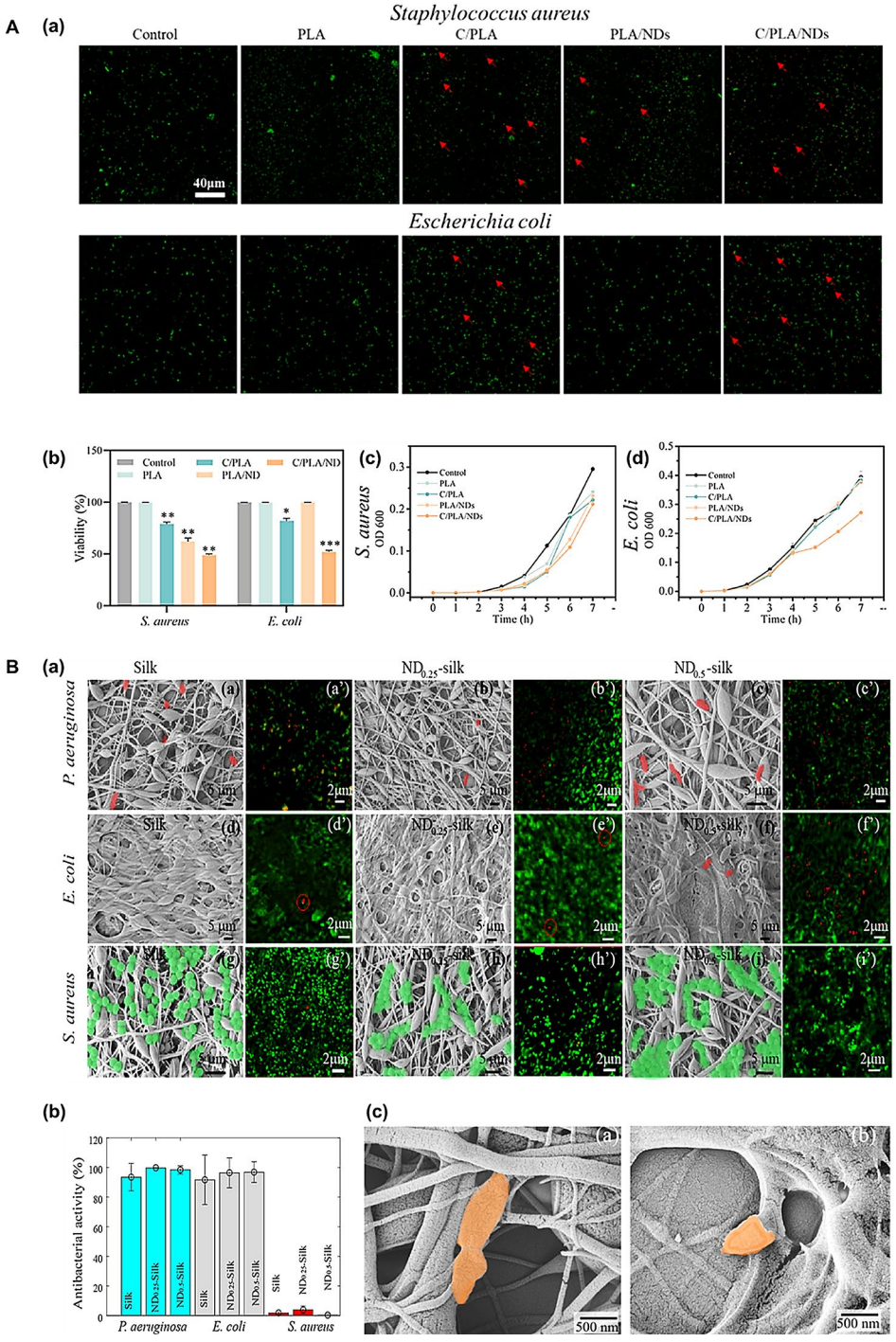

Fig. 12 (**A**): After 7 h of cultivation of *S. aureus* and *E. coli* in the scaffolds and their (a) Live/dead images (b) Viability graph (c) and (d) Proliferation graph. Reproduced with permission [168]. (**B**): (a) Antibacterial activity of silk and ND-silk nanofibers against *P. aeruginosa*, *E. coli* and *S. aureus*, (b) Antibacterial activity, and (c) SEM images of damaged *P. aeruginosa* and *E. coli*. Reproduced with permission [169]

TFC-EtOH (treated with ethanol) were also fabricated. The scaffolds were exposed to *E. coli* cultures for 3 h to evaluate their antibacterial efficiency (Fig. 13A-a). Colony plating analysis (Fig. 13A-b and e) revealed bacterial mortality rates of 52.4%, 59.7%, and 63.7% for TFC-250, TFC-500, and TFC-1000, respectively, while TFC-0 and TFC-EtOH showed significantly lower mortality rates of 1.3% and 14%. Confocal microscopy analysis further confirmed these findings, showing mortality rates of 48.3%, 51.9%, and 52.1% for TFC-250, TFC-500, and TFC-1000, while TFC-0 and TFC-EtOH exhibited negligible bacterial inhibition (Fig. 13A-c and f). These results highlight

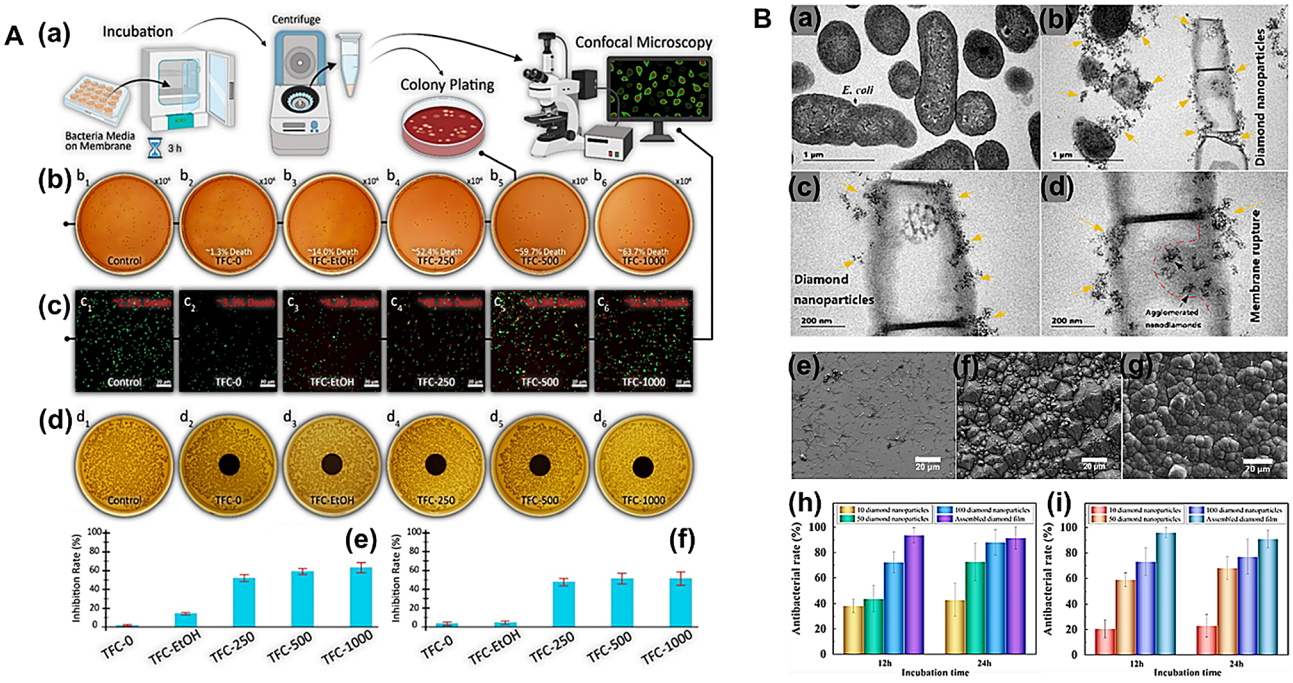

Fig. 13 (**A**): (a) Schematic illustrating the preparation steps for colony plating and confocal microscopy tests. (b) Results of the colony plating tests. (c) Results of the confocal microscopy analysis. (d) Images from the inhibition zone assay. Bacterial inhibition rates from (e) colony plating and (f) confocal microscopy tests. Reproduced with permission [20]. (**B**): TEM images of (a) untreated *E.coli* and (b), (c), (d) *E.coli* treated with ND particles. Adhesion images of *Bacillus sp.* on (e) silicon wafer and (f) ND support, and (g) *E.coli* on ND support. Antibacterial rates of (h) *Bacillus sp.* and (i) *E.coli*. Reproduced with permission [171]

the significant improvement in bacterial inactivation rates due to the presence of ND particles. The disk inhibition zone test also supported the antibacterial activity of the ND-based scaffolds. As shown in Fig. 13A-d, none of ND-EDA-containing scaffolds exhibited inhibition zones, indicating that the ND particles were strongly bonded to the polyamide layer. This strong binding is crucial for long-term activity in anti-biofouling applications. Hence, in this study, ND-EDA-based TFC scaffolds not only enhance antibacterial activity but also demonstrate long-term effectiveness in the presence of bacteria [20]. Similarly, Conceição et al. developed a DLC + ND platform by coating Ti6Al4V with diamond-like carbon (DLC) and doping it with 1%w/v ND. The antibacterial properties of this platform were tested by direct exposure to *E. coli* for 6 h. As a result, the pure DLC platform demonstrated approximately 30% growth inhibition, whereas the DLC + ND platform achieved a significantly higher inhibition rate of around 95%. This remarkable antibacterial effect is attributed to the mechanism by which ND particles interact with the bacterial cell wall. ND particles attach to and disrupt the cell wall, subsequently penetrating the cell to damage DNA and induce oxidative stress, ultimately leading to bacterial cell death. The potent antibacterial activity of the DLC + ND platform highlights its potential for applications in wound healing [170]. Shen et al. developed micro/nano support structures using hydroxylated silicon wafers and carbonylated ND. First, testing the antimicrobial effect of ND particles showed that compared to untreated *E. coli* (Fig. 13B-a), ND particles adhered to the surface of *E. coli* influenced bacterial membrane permeability (Fig. 13B-b). As a result, the exposure of bacterial cell walls to ND particles caused damage and rupture of the bacterial membrane, releasing cytoplasmic contents (Fig. 13B-c and d). To evaluate the antimicrobial efficiency of the support, *E. coli* and *Bacillus sp.* were cultured for 2 days. Observations showed clear adhesion and colony formation on the silicon wafer surface (Fig. 13B-e). In contrast, very little attachment of bacteria was observed on the ND support (Fig. 13B-f and g). The analysis of antibacterial rate revealed that the ND support exhibited a higher effect compared to ND particles alone (Fig. 13B-h and i), suggesting that ND support possesses superior antibacterial properties, effectively inhibiting bacterial attachment and colonization for high potential applications in biomedical settings [171].

Biological effects and wound healing

ND-based nanofibers promote wound healing by enhancing cell adhesion, proliferation, and migration, mimicking the extracellular matrix (ECM). They maintain optimal moisture levels, prevent infections with antibacterial properties, and support tissue regeneration, making them ideal for advanced wound care [9, 172]. For instance,

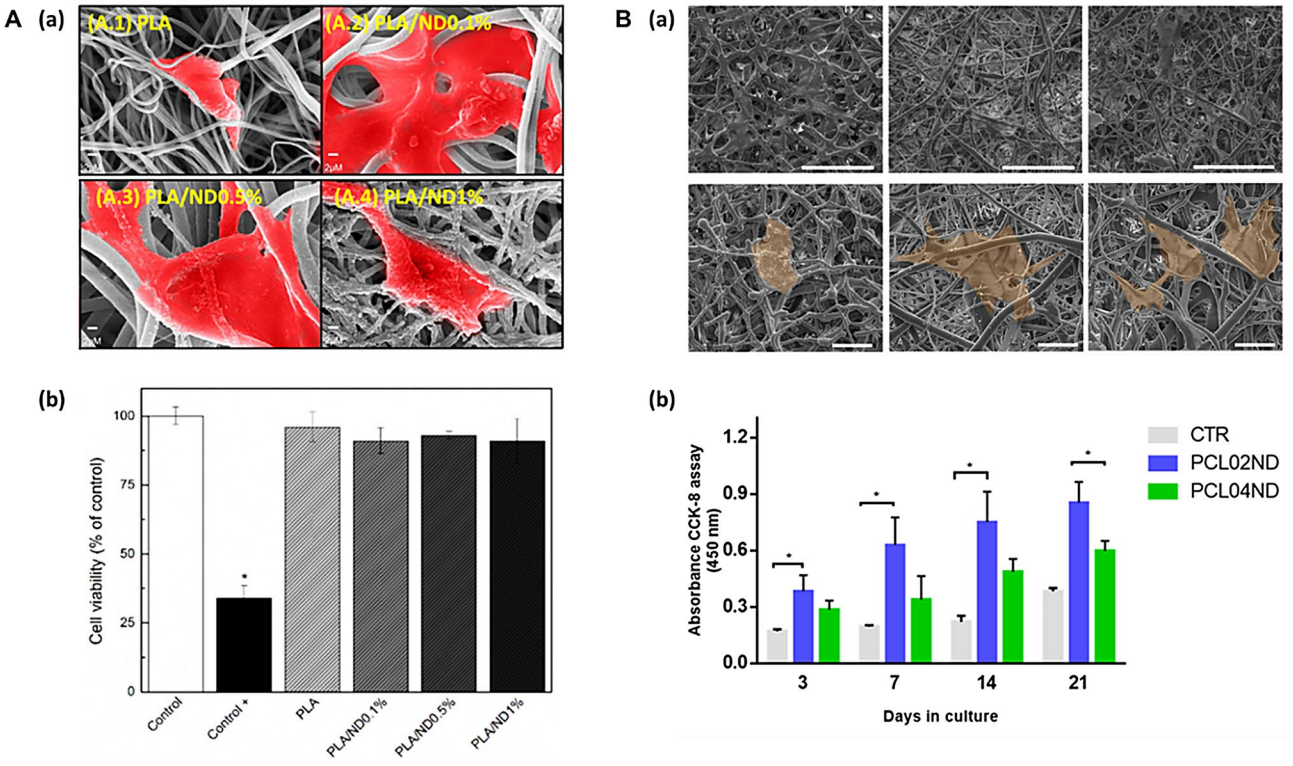

Fig. 14 (**A**): (a) Adhesion and (b) viability of L929 cells after 24 h with scaffolds. Reproduced with permission [44]. (**B**): (a) SEM images of hMSCs adhered to the nanofibers after 24 h (from left to right: PCL and fND/PCL 0.2wt%) (Top: low magnification, scale bar 100 µm; Bottom: high magnification, scale bar 20 µm). (b) Graph of hMSC viability on nanofibers up to 21 days. Reproduced with permission [173]

Pereira and group checked the biocompatibility of PLA/ND nanofibers [44]. For this, they fabricated PLA, PLA/ND 0.1%, PLA/ND 0.5%, and PLA/ND 1% nanofibers by blending poly(lactic acid) (PLA) with ND at concentrations of 0.1%, 0.5% and 1%. As shown in Fig. 14A-b, cytotoxicity analysis using L929 fibroblasts revealed no toxicity in any of the samples after 24 h. Furthermore, cell adhesion experiments demonstrated that the PLA/ND 0.1% and PLA/ND 0.5% nanofibers exhibited superior adhesion and spreading compared to pure PLA (Fig. 14A-a). This improvement is attributed to the decoration of nanofiber walls by ND, forming nanostructured pore walls that enhance the potential for cell growth. The excellent cell adhesion and spreading properties of PLA/ND nanofibers suggest their potential as effective scaffolds in wound healing applications. The nanostructural characteristics and increased surface area of ND promote cell growth at the wound site, accelerate tissue regeneration, and improve biocompatibility, thereby contributing to enhanced wound healing outcomes. In a study performed by Guarino and team, they used fluorescent ND (0.2wt% and 0.4wt%) with PCL to evaluate the response of nanofibers on hBMSCs. SEM images of 24 h culture showed no cytotoxicity, and excellent cell adhesion [173]. In particular, ND-containing nanofibers exhibited more pronounced filopodia at the fiber surface boundary as demonstrated in Fig. 14B-a. This was attributed to the increase in the hydrophilicity and surface energy of the nanofibers due to the presence of ND, which effectively enhanced the initial cell adhesion and protein adsorption phases. Additionally, Fig. 14B-b shows significant improvement in cell viability for up to 14 days in the presence of ND with increase in cellular response compared to pure PCL nanofibers up to 21 days. These results indicate that the addition of ND does not hinder the biological response of cells but rather supports cell adhesion and survival by mimicking the extracellular matrix (ECM) fiber structure with the unique morphology of the nanofibers. This characteristic suggests that the nanofibers could potentially act as a scaffold to accelerate cell proliferation and tissue regeneration at wound sites, thus maximizing healing effects.

Mahdavi et al. developed nanofibers with physical and mechanical properties similar to those of natural skin by incorporating chitosan/bacterial cellulose (CS/BC) and medical grade ND (MND) [42]. MND was included in concentrations of 0%, 1%, 2%, and 3%, resulting in the samples ND0, ND1, ND2, and ND3. The nanofibers containing MND showed improvements in tensile strength and elasticity, while permeability decreased. This suggests that the addition of MND enhances the protective capability of the nanofibers, potentially helping to

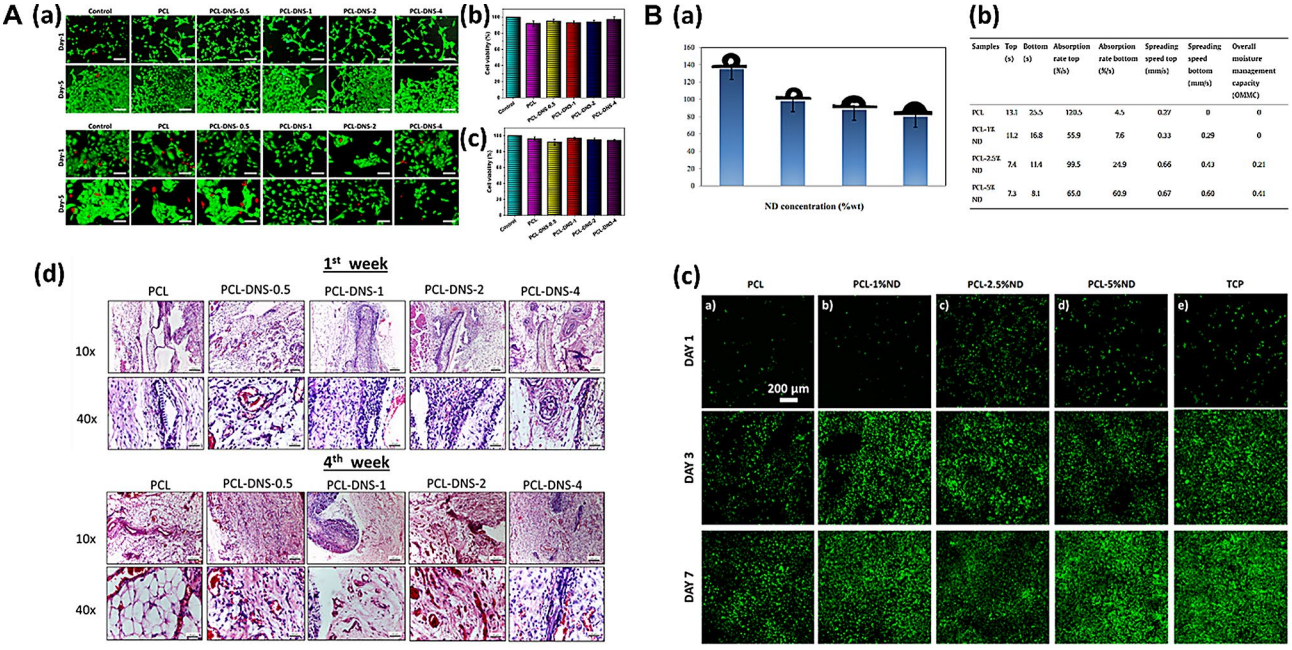

Fig. 15 (**A**): (a) 3T3 fibroblast and HaCaT keratinocyte cell morphology after 1, and 5 days of culture. MTT assay for cell viability for (b) 3T3 fibroblasts and (c) HaCaT keratinocytes. (d) H&E staining microscopic images of PCL and PCL-DNS scaffolds implanted for 1 and 4 weeks. Reproduced with permission [174]. (**B**): (a) Contact angle of PCL-ND nanofibers. (b) Moisture management characteristics of PCL-ND nanofibers. (c) Green fluorescent protein images of CHO cells seeded on nanofibers after 1, 3, and 7 days. Reproduced with permission [175]

prevent infections and safely protect wound sites. Additionally, when evaluating the cell viability of L929 fibroblasts, which are relevant to wound healing, after 24 and 72 h, the MND-containing nanofibers maintained high levels of viability compared to the control. These results indicate that the MND-containing nanofibers offer excellent biocompatibility and effectiveness in wound healing environments. In another study, Augustine et al. fabricated diamond nanosheets (DNS) using ND and mixed them with PCL at concentrations of 0.5%, 1%, 2%, and 4% to create PCL-DNS-0.5, PCL-DNS-1, PCL-DNS-2, and PCL-DNS-4 nanofibers [174]. They then evaluated the cell compatibility of the nanofibers using human keratinocyte (HaCaT) cells and mouse fibroblasts (3T3 cells). The results showed that both cell types exhibited fewer dead cells in the PCL-DNS nanofibers compared to the control and pure PCL groups (Fig. 15A-a). Additionally, as shown in the Fig. 15A-b and c, MTT cell viability assays confirmed that incorporating DNS into the nanofibers did not induce cell toxicity. In vivo biocompatibility was assessed by subcutaneously implanting the nanofibers into mice for 4 weeks and analyzing local tissue response through histopathological examination. The results showed that the PCL-DNS nanofibers supported blood vessel formation, as evidenced by the presence of RBCs (pink/red cells) one week after implantation (Fig. 15A-d). These findings suggest that the high surface area and tunable surface chemistry of ND may promote cell growth and tissue regeneration in PCL-DNS scaffolds, aiding in wound healing. Similarly, Houshyar et al. also fabricated PCL-based nanofibers containing ND at concentrations of 1%w/w, 2.5%w/w and 5%w/w, naming them PCL-1%ND, PCL-2.5%ND, PCL-5%ND, respectively [175]. As shown in Fig. 15B-a, contact angle measurements of the PCL-ND nanocomposites showed that the contact angles for PCL-1%ND, PCL-2.5%ND, and PCL-5%ND were 98°, 88°, and 80°, respectively, demonstrating a significant decrease as the ND concentration increased. Analysis of the moisture management properties revealed that higher ND content in the nanofibers improved liquid transfer from the upper to the lower layer, enhancing moisture regulation. Notably, PCL-5%ND exhibited a 51% improvement in overall moisture management compared to pure PCL nanofibers (Fig. 15B-b). These properties are crucial for providing appropriate moisture to the wound area, preventing excessive dryness, and facilitating the removal of excess liquid, thereby supporting the wound healing process. Furthermore, in cell culture experiments using Chinese hamster ovarian (CHO) cells, the cell viability after 1, 3, and 7 days of incubation increased with higher ND concentrations, along with a gradual rise in cell density (Fig. 15B-c). This indicates that ND enhances the hydrophilicity of PCL, promoting cell proliferation. These findings suggest that ND-based nanofibers are a suitable option for addressing the challenges of complex wound management.

Conclusion and future perspective

Nanodiamonds (NDs) have emerged as a very promising material for enhancing the performance of electrospun nanofibers for biomedical applications, particularly within the realm of wound healing. Their ability to mimic the extracellular matrix (ECM), together with intrinsic antibacterial properties, holds a lot of promise for addressing fundamental challenges in tissue regeneration. However, several major hurdles should be overcome before the successful clinical application of ND-based nanofibers. These encompass the need for economically viable and scalable synthesis protocols, methods to inhibit ND aggregation, rigorous evaluation of biocompatibility, and enhancement of long-term material stability and antimicrobial efficacy. It is crucial to overcome these challenges to enable the translation of the beneficial characteristics of ND-based nanofibers into relevant clinical applications. Beyond wound healing, the prospective reach of ND-based nanofibers substantially covers numerous fields in biomedical engineering. Their unique combination of mechanical strength, biocompatibility, and surface modifiability renders them versatile devices with diverse applications in fields including tissue engineering, drug delivery, biosensing, orthopedic, and ophthalmic devices.

Optimization of the synthesis techniques of NDs, such as chemical vapor deposition and plasma-assisted synthesis, to be more scalable and cost-effective is the scope of future research. Surface functionalization processes such as carboxylation, hydroxylation, and biocompatible coatings such as PEG are required for enhancing the dispersion of NDs and minimizing cytotoxicity. Additionally, extensive in vitro experiments and in vivo experiments need to be conducted to fully assess the biocompatibility and long-term stability of nanofibers from nanoparticles under physiological conditions. Of particular interest are investigations on hybrid scaffolds and cross-linked polymer-nanoparticle composites to enhance the mechanical properties and longevity of these materials. Continued development of sophisticated dispersion methods, including ultrasonication and shear-assisted mixing, will facilitate uniform distribution of nanoparticles into the nanofibers. Furthermore, research needs to be conducted on integrating bioactive molecules and growth factors into nanofibers derived from natural sources to further accelerate tissue regeneration and wound healing.

Successful fabrication of ND-based nanofibers has the potential to greatly impact the broader field of biomedical engineering. In tissue engineering and drug delivery, they can serve as improved scaffolds, mimicking the ECM and offering mechanical support for complex tissue regeneration and offer localized and controlled release of therapeutics, including gene therapy. Their better surface properties enable the development of very sensitive biosensors for the diagnosis of diseases at early stages and also for continuous monitoring. Additionally, in orthopedic applications, they can promote osseointegration of implants and bone regeneration. By capitalizing on their exceptional properties and modifying their function using surface treatments and composite architecture, researchers are designing novel solutions for overcoming key clinical problems and enhancing patient outcomes, advancing ND-based nanofibers from the status of laboratory phenomenon to the level of clinical reality.

Author contributions

H.P. and T.V.P. - Conceptualization, Supervision, Visualization, Writing original draft, and supervising. K.T.L.- Conceptualization, Funding acquisition, Supervision and Validation. C.M. - Supervision, Validation.

Funding

This work was supported by the Innovative Human Resource Development for Local Intellectualization program through the Institute of Information & Communications Technology Planning & Evaluation (IITP) grant funded by the Korea government (MSIT)(IITP-2025-RS-2023-00260267).

Data availability

No datasets were generated or analysed during the current study.

Declarations

Ethics approval and consent to participate

Not applicable.

Competing interests

The authors declare no competing interests.

Received: 11 February 2025 / Accepted: 24 March 2025
Published online: 09 April 2025

References

1. Hyder A, Ali A, Buledi JA, Memon AA, Iqbal M, Bangalni TH, Solangi AR, Thebo KH. Akhtar, nanodiamonds: A Cutting-Edge approach to enhancing biomedical therapies and diagnostics in biosensing. Chem Record. 2024;24(4):e202400006.
2. Alexander E, Leong KW. Nanodiamonds in biomedical research: therapeutic applications and beyond. PNAS Nexus. 2024;3(5):198
3. Lee JH, Loh ND, Yeo ZY, Ong YK, Balakrishnan D, Limpo CMA, et al. Engineering a hierarchy of disorder: A new route to synthesize High-Performance 3D nanoporous All-Carbon materials. Adv Mater. 2024;36(32):2402628. https://doi.org/10.1002/adma.202402628
4. Jariwala DH, Patel D, Wairkar S. Surface functionalization of nanodiamonds for biomedical applications. Mater Sci Engineering: C. 2020;113:110996.
5. Barzegar Amiri Olia M, Donnelly PS, Hollenberg LC, Mulvaney P, Simpson DA. Advances in the surface functionalization of nanodiamonds for biological applications: A review. ACS Appl Nano Mater. 2021;4(10):9985–10005.
6. Qin J-X, Yang X-G, Lv C-F, Li Y-Z, Liu K-K, Zang J-H, Yang X, Dong L. Shan, nanodiamonds: synthesis, properties, and applications in nanomedicine. Mater Design. 2021;210:110091.
7. Kausar A. Nanodiamond reinforcement effects in thermosetting matrices—design, functional features and significance. J Macromolecular Sci Part A. 2024;61(10):724–41.
8. Saba T, Saad KSK, Rashid AB. Precise surface engineering: leveraging chemical vapor deposition for enhanced biocompatibility and durability in biomedical implants. Heliyon 10(18) (2024).
9. Adel M, Keyhanvar P, Zare I, Tavangari Z, Akbarzadeh A, Zahmatkeshan M. Nanodiamonds for tissue engineering and regeneration. J Drug Deliv Sci Technol. 2023;90:105130.

10. Ghajarieh A, Habibi S, Talebian A. Biomedical applications of nanofibers. Russ J Appl Chem. 2021;94(7):847–72.
11. Mirhaj M, Tavakoli M, Varshosaz J, Labbaf S, Jafarpour F, Ahmaditabar P, Salehi S, Kazemi N. Platelet rich fibrin containing nanofibrous dressing for wound healing application: fabrication, characterization and biological evaluations. Biomaterials Adv. 2022;134:112541.
12. Mirhaj M, Salehi S, Tavakoli M, Varshosaz J, Labbaf S, Abadi SAM, Haghighi V. Comparison of physical, mechanical and biological effects of leucocyte-PRF and advanced-PRF on polyacrylamide nanofiber wound dressings: in vitro and in vivo evaluations. Biomaterials Adv. 2022;141:213082.
13. Mirhaj M, Varshosaz J, Labbaf S, Emadi R, Seifalian AM, Sharifianjazi F, Tavakoli M. Mupirocin loaded core-shell pluronic-pectin-keratin nanofibers improve human keratinocytes behavior, angiogenic activity and wound healing. Int J Biol Macromol. 2023;253:126700.
14. Tavakoli M, Mirhaj M, Salehi S, Varshosaz J, Labbaf S, Golshirazi A, Kazemi N, Haghighi V. Coaxial electrospun angiogenic nanofiber wound dressing containing advanced platelet rich-fibrin. Int J Biol Macromol. 2022;222:1605–18.
15. Alizadeh M, Salehi S, Tavakoli M, Mirhaj M, Varshosaz J, Kazemi N, Salehi S, Mehrjoo M, Abadi SAM. PDGF and VEGF-releasing bi-layer wound dressing made of sodium tripolyphosphate crosslinked gelatin-sponge layer and a Carrageenan nanofiber layer. Int J Biol Macromol. 2023;233:123491.
16. Mirhaj M, Varshosaz J, Nasab PM, Al-Musawi MH, Almajidi YQ, Shahriari-Khalaji M, Tavakoli M, Alizadeh M, Sharifianjazi F, Mehrjoo M, Labbaf S, Sattar M, Esfahani SN. A double-layer cellulose/pectin-soy protein isolate-pomegranate Peel extract micro/nanofiber dressing for acceleration of wound healing. Int J Biol Macromol. 2024;255:128198.
17. Mirhaj M, Varshosaz J, Labbaf S, Emadi R, Marcus Seifalian A, Sharifianjazi F. An antibacterial Multi-Layered scaffold fabricated by 3D printing and electrospinning methodologies for skin tissue regeneration. Int J Pharm. 2023;645:123357.
18. Tavakoli M, Mirhaj M, Varshosaz J, Salehi S, Mohanna SM, Salehi S, Haghighi V, Kazemi N, Mehrjoo M, Shahriari-Khalaji M. Asymmetric tri-layer sponge-nanofiber wound dressing containing insulin-like growth factor-1 and multi-walled carbon nanotubes for acceleration of full-thickness wound healing. Biomaterials Adv. 2023;151:213468.
19. Park H, Patil TV, Dutta SD, Lee J, Ganguly K, Randhawa A, Kim H, Lim KT. Extracellular Matrix-Bioinspired anisotropic topographical cues of electrospun nanofibers: a strategy of wound healing through macrophage polarization. Adv Healthc Mater. 2024;13(12):2304114.
20. Karami P, Aktij SA, Khorshidi B, Firouzjaei MD, Asad A, Elliott M, Rahimpour A, Soares JB, Sadrzadeh M. Nanodiamond-decorated thin film composite membranes with antifouling and antibacterial properties. Desalination. 2022;522:115436.
21. Antal TK, Volgusheva AA, Baizhumanov AA, Kukarskikh GP, Mezzi A, Caschera D, Ciasca G, Lambreva MD. Nanodiamond particles reduce oxidative stress induced by Methyl viologen and high light in the green Alga chlamydomonas reinhardtii. Int J Mol Sci. 2023;24(6):5615.
22. Luo X, Zhang H, Cao Z, Cai N, Xue Y, Yu F. A simple route to develop transparent doxorubicin-loaded nanodiamonds/cellulose nanocomposite membranes as potential wound dressings. Carbohydr Polym. 2016;143:231–8.
23. Chauhan S, Jain N, Nagaich U. Nanodiamonds with powerful ability for drug delivery and biomedical applications: recent updates on in vivo study and patents. J Pharm Anal. 2020;10(1):1–12.
24. Kausar A. Carbonaceous nanofillers in polymer matrix, Polymeric Nanocomposites with Carbonaceous Nanofillers for Aerospace Applications (2022) 23.
25. Li Z, Wang Y, Ma M, Ma H, Hu W, Zhang X, Zhuge Z, Zhang S, Luo K, Gao Y. Ultrastrong conductive in situ composite composed of nanodiamond incoherently embedded in disordered multilayer graphene. Nat Mater. 2023;22(1):42–9.
26. Thekkedath A, Sridharan K. Nanodiamonds and its applications. Applications and Use of Diamond; 2022.
27. Kumar S, Nehra M, Kedia D, Dilbaghi N, Tankeshwar K, Kim K-H. Nanodiamonds: emerging face of future nanotechnology. Carbon. 2019;143:678–99.
28. Mumtaz M, Hussain N, Salam S, Bilal M. Multifunctional nanodiamonds as emerging platforms for cancer treatment, and targeted delivery of genetic factors and protein medications—a review. J Mater Sci. 2022;57(17):8064–99.
29. Arun Kumar M, Selvaraj SK, Kanniyappan S, Karthikeyan B, Chadha U. Effects of adding nanodiamonds in mechanical properties of jute and Ramie fiber reinforced epoxy composites. Polym Compos. 2024;45:11872.
30. Reina G, Zhao L, Bianco A, Komatsu N. Chemical functionalization of nanodiamonds: opportunities and challenges ahead. Angew Chem Int Ed. 2019;58(50):17918–29.
31. Rao RN, Albaseer SS. Nanomaterials in chromatographic sample preparations, Nanomaterials in Chromatography, Elsevier2018, pp. 201–231.
32. Mochalin V, Shenderova O, Ho D, Gogotsi Y. The properties and applications of nanodiamonds. Nano-enabled Med Appl. 2020;7(1):313–50.
33. Yang N, Yu S, Macpherson JV, Einaga Y, Zhao H, Zhao G, et al. Conductive diamond: synthesis, properties, and electrochemical applications. Chem Soc Rev. 2019;48(1):157–204.
34. Boey JY, Lee CK, Tay GS. Factors affecting mechanical properties of reinforced bioplastics: a review. Polymers. 2022;14(18):3737.
35. Bhattacharyya A, Priya VK, Kim J-h, Khatun MR, Nagarajan R, Noh I. Nanodiamond enhanced mechanical and biological properties of extrudable gelatin hydrogel cross-linked with Tannic acid and ferrous sulphate. Biomaterials Res. 2022;26(1):37.
36. Morimune-Moriya S, Salajkova M, Zhou Q, Nishino T, Berglund LA. Reinforcement effects from nanodiamond in cellulose nanofibril films. Biomacromolecules. 2018;19(7):2423–31.
37. Adhikari P, Jani PK, Hsiao LC, Rojas OJ, Khan SA. Interfacial contributions in nanodiamond-reinforced polymeric fibers. J Phys Chem B. 2021;125(36):10312–23.
38. Junzhuo W, Shijia G, Hui Y, Jianlin L, Lianjun W, Wan J. Robust natural graphite-based bulk graphites with nanodiamond-containing fibrous nanofiller as reinforcement by electrohydrodynamic processing. Ceram Int. 2024;50(13):24387–96.
39. Hinzmann C, Parsons DF, Fiedler J, Zalieckas J, Holst B. Nanodiamond-treated flax: improving properties of natural fibers. Cellulose. 2024;31(1):685–701.
40. Morimune-Moriya S, Yada S, Kuroki N, Ito S, Hashimoto T, Nishino T. Strong reinforcement effects of nanodiamond on mechanical and thermal properties of polyamide 66. Compos Sci Technol. 2020;199:108356.
41. Mostafavi Yazdi SJ, Baqersad J. Mechanical modeling and characterization of human skin: A review. J Biomech. 2022;130:110864.
42. Mahdavi M, Mahmoudi N, Rezaie Anaran F, Simchi A. Electrospinning of nanodiamond-modified polysaccharide nanofibers with physico-mechanical properties close to natural skins. Mar Drugs. 2016;14(7):128.
43. Cai N, Dai Q, Wang Z, Luo X, Xue Y, Yu F. Preparation and properties of nanodiamond/poly(lactic acid) composite nanofiber scaffolds. Fibers Polym. 2014;15(12):2544–52.
44. Pereira F, Salles G, Rodrigues B, Marciano F, Pacheco-Soares C, Lobo A. Diamond nanoparticles into Poly (lactic acid) electrospun fibers: cytocompatible and bioactive scaffolds with enhanced wettability and cell adhesion. Mater Lett. 2016;183:420–4.
45. Carbon D-L, Diamond. Carbon Nanotubes and Graphene for Biomedical Applications, (2019).
46. Mayerhoefer E, Krueger A. Surface control of Nanodiamond: from homogeneous termination to complex functional architectures for biomedical applications. Acc Chem Res. 2022;55(24):3594–604.
47. Kabir II, Osborn JC, Lu W, Mata JP, Rehm C, Yeoh GH, Ersez T. Structure evolution of nanodiamond aggregates: a SANS and USANS study. J Appl Crystallogr. 2022;55(2):353–61.
48. Taylor AC, González CH, Miller BS, Edgington RJ, Ferretti P, Jackman RB. Surface functionalisation of nanodiamonds for human neural stem cell adhesion and proliferation. Sci Rep. 2017;7(1):7307.
49. Khan M, Hamid A, Tiehu L, Zada A, Attique F, Ahmad N, Ullah A, Hayat A, Mahmood I, Hussain A. Surface optimization of detonation nanodiamonds for the enhanced mechanical properties of polymer/nanodiamond composites. Diam Relat Mater. 2020;107:107897.
50. Elunina K, Kudryashova O, Petrov E, Influence of Ultrasonic Treatment on the Microstructure of Particles of Detonation Synthesis Nanodiamonds, 2021 IEEE 22nd International Conference of Young Professionals in Electron Devices and, Materials. (EDM), IEEE, 2021, pp. 243–246.
51. Turcheniuk K, Mochalin VN. Biomedical applications of nanodiamond. Nanotechnology. 2017;28(25):252001.
52. Quan C, Lin H, Xiao H, Zhao J. Inhibitory effect of carboxylated nanodiamond on oral pathogenic bacteria Streptococcus mutans. J Clin Lab Anal. 2021;35(8):e23872.
53. Santacruz-Gomez K, Sarabia-Sainz A, Acosta-Elias M, Sarabia-Sainz M, Janetanakit W, Khosla N, Melendrez R, Montero MP, Lal R. Antioxidant activity of hydrated carboxylated nanodiamonds and its influence on water γ-radiolysis. Nanotechnology. 2018;29(12):125707.
54. Ashek-I-Ahmed L, Gines S, Mandal C-Y, Song OA, Williams MN, Sarmiento C-L, Cheng. Facile amine termination of nanodiamond particles and their surface reaction dynamics. ACS Omega. 2019;4(16):16715–23.

55. Mangal U, Seo J-Y, Yu J, Kwon J-S, Choi S-H. Incorporating aminated nanodiamonds to improve the mechanical properties of 3D-printed resin-based biomedical appliances. Nanomaterials. 2020;10(5):827.
56. Zhao N, Song M, Zhang X, Xu W, Liu X. Nanodiamond Coating in Energy and Engineering Fields: Synthesis Methods, Characteristics, and Applications, Small (2024) 2401292.
57. Ekimov E, Shiryaev AA, Grigoriev Y, Averin A, Shagieva E, Stehlik S, Kondrin M. Size-dependent thermal stability and optical properties of ultra-small nanodiamonds synthesized under high pressure. Nanomaterials. 2022;12(3):351.
58. Lu F, Wei C, Yin X, Kang L, Zhu M, Dai B. The effect of sp2 content in carbon on its catalytic activity for acetylene hydrochlorination. Nanomaterials. 2022;12(15):2619.
59. Arnault J. Surface modifications of nanodiamonds and current issues for their biomedical applications, Novel aspects of diamond: From growth to applications (2019) 415–460.
60. Li Y, He S, Zhou Z, Zhou S, Huang S, Fane AG, Zheng C, Zhang Y, Zhao S. Carboxylated Nanodiamond-enhanced photocatalytic membranes with improved antifouling and self-cleaning properties. Ind Eng Chem Res. 2020;59(8):3538–49.
61. Yang T-C, Chang C-Y, Yarmishyn AA, Mao Y-S, Yang Y-P, Wang M-L, Hsu C-C, Yang H-Y, Hwang D-K, Chen S-J. Carboxylated nanodiamond-mediated CRISPR-Cas9 delivery of human retinoschisis mutation into human iPSCs and mouse retina. Acta Biomater. 2020;101:484–94.
62. Hou Z, Wang Z, Wang P, Chen F, Luo X. Near-infrared light-triggered mild-temperature photothermal effect of nanodiamond with functional groups. Diam Relat Mater. 2022;123:108831.
63. Zandieh M, Liu J, Metal-Mediated DNA. Adsorption on carboxylated, hydroxylated, and hydrogenated nanodiamonds. Langmuir. 2023;39(33):11596–602.
64. Pan X, Zhang Y, Zhang Y, Yang M, Yang Z, Liu Y, Zhang P, Han Z, Wang X, Fu Y. Monodispersed nanodiamonds for enhanced anticorrosion of waterborne epoxy coatings. Ind Eng Chem Res. 2023;63(1):307–17.
65. Shuai C, Li Y, Wang G, Yang W, Peng S, Feng P. Surface modification of Nanodiamond: toward the dispersion of reinforced phase in poly-l-lactic acid scaffolds. Int J Biol Macromol. 2019;126:1116–24.
66. Wen Z, Wu J, Fan G. Facile fabrication of rhodium/nanodiamond hybrid as advanced catalyst toward hydrogen production from ammonia–borane. Catalysts. 2020;10(9):1037.
67. Jirásek V, Stehlík Š, Štenclová P, Artemenko A, Rezek B, Kromka A. Hydroxylation and self-assembly of colloidal hydrogenated nanodiamonds by aqueous oxygen radicals from atmospheric pressure plasma jet. RSC Adv. 2018;8(66):37681–92.
68. Kord Forooshani P, Pinnaratip R, Polega E, Tyo AG, Pearson E, Liu B, Folayan T-O, Pan L, Rajachar RM, Heldt CL. Hydroxyl radical generation through the Fenton-like reaction of hematin-and catechol-functionalized microgels. Chem Mater. 2020;32(19):8182–94.
69 Tsuneda T. Fenton reaction mechanism generating no OH radicals in Nafion membrane decomposition. Sci Rep. 2020;10(1):18144.
70. Zhong H, Wang Q, Qu J, Li X, Mukerabigwi JF, Asibaike L, Fang Y, Cao Y. Dispersion of reduced nanodiamond and its application in lubrication. Mater Today Commun. 2023;37:106999.
71. Lim DG, Kang E, Jeong SH. pH-dependent nanodiamonds enhance the mechanical properties of 3D-printed hyaluronic acid nanocomposite hydrogels. J Nanobiotechnol. 2020;18:1–10.
72. Chi Q, Chen D, Wang X, Zhang C, Zhang T, Wu G, Tang C. Improvement of thermal conductivity properties of epoxy resin by constructing sesame cookie-like nanodiamond-boron nitride, Polymer Composites.
73. Gulka M, Balasubramanian P, Shagieva E, Copak J, Khun J, Scholtz V, Jelezko F, Stehlik S, Cigler P. Surface optimization of nanodiamonds using non-thermal plasma. Carbon. 2024;224:119062.
74. He Y, Chang Q, Lu F. Oxygen-releasing biomaterials for chronic wounds breathing: from theoretical mechanism to application prospect. Mater Today Bio. 2023;20:100687.
75. Gim G, Haider Z, Suh S-I, Ahn Y-Y, Kim K, Kim E-J, Lee H, Kim H-i, Lee J. Low-temperature hydrogenation of nanodiamond as a strategy to fabricate sp3-hybridized nanocarbon as a high-performance persulfate activator. Appl Catal B. 2022;316:121589.
76. Stehlik S, Szabo O, Shagieva E, Miliaieva D, Kromka A, Nemeckova Z, Henych J, Kozempel J, Ekimov E, Rezek B. Electrical and colloidal properties of hydrogenated nanodiamonds: effects of structure, composition and size. Carbon Trends. 2024;14:100327.
77. Ducrozet F, Brun E, Girard HA, Arnault J-C, Sicard-Roselli C. Milled nanodiamonds overproduce solvated electrons while scavenging hydroxyl radicals under gamma irradiation. J Phys Chem C. 2023;127(39):19544–53.
78. Tang G, Zhang M, Liu Q, Tian X, Mai R. Applications of nanodiamonds in the diagnosis and treatment of neurological diseases. J Nanopart Res. 2022;24(3):55.
79. Kulakova I, Pereyaslavcev AY, Lisichkin G. Regularities of chlorination of the detonation nanodiamond surface. Mosc Univ Chem Bull. 2019;74:246–56.
80. Basso L, Cazzanelli M, Orlandi M, Miotello A. Nanodiamonds: synthesis and application in sensing, catalysis, and the possible connection with some processes occurring in space. Appl Sci. 2020;10(12):4094.
81. Singh D, Ray S. A short appraisal of nanodiamonds in drug delivery and targeting: recent advancements. Front Nanatechnol. 2023;5.
82. Alwani S, Hua Q, Iftikhar S, Appathurai NP, Michel D, Karunakaran C, Badea I. Lysine functionalized nanodiamonds as gene carriers-Investigation of internalization pathways and intracellular trafficking. Diam Relat Mater. 2019;98:107477.
83. Ryu TK, Baek SW, Kang RH, Choi SW. Selective photothermal tumor therapy using nanodiamond-based nanoclusters with folic acid. Adv Funct Mater. 2016;26(35):6428–36.
84. Li A, Wang H, Liu X, Shen W, Fang C, Zhang Z, Zhang Y, Chen L, Wang Q, Wan B, Wang Y, Shan C. Enhanced stability of sodium anodes by amino-functioned macroporous two-dimensional nanodiamond coated polypropylene separators. Chem Eng J. 2024;491:151914.
85. Dey T, Ghosh A, Sanyal A, Charles CJ, Pokharel S, Nair L, Singh M, Kaity S, Ravichandiran V, Kaur K. Surface engineered nanodiamonds: mechanistic intervention in biomedical applications for diagnosis and treatment of cancer. Biomed Mater. 2024;19(3):032003.
86. Jung H-S, Neuman KC. Surface modification of fluorescent nanodiamonds for biological applications. Nanomaterials. 2021;11(1):153.
87. Ekimov E, Lyapin S, Grigoriev YV, Zibrov I, Kondrina K. Size-controllable synthesis of ultrasmall diamonds from halogenated Adamantanes at high static pressure. Carbon. 2019;150:436–8.
88. Ekimov E, Shiryaev A, Sidorov V, Grigoriev Y, Averin A, Kondrin M. Synthesis and properties of nanodiamonds produced by HPHT carbonization of 1-fluoroadamantane. Diam Relat Mater. 2023;136:109907.
89. Zhou J, Laube C, Knolle W, Naumov S, Prager A, Kopinke F-D, Abel B. Efficient Chlorine atom functionalization at nanodiamond surfaces by electron beam irradiation. Diam Relat Mater. 2018;82:150–9.
90. Luo Z, Wan Q, Yu Z, Lin S, Xie Z, Wang X. Photo-fluorination of nanodiamonds catalyzing oxidative dehydrogenation reaction of ethylbenzene. Nat Commun. 2021;12(1):6542.
91. Chen L, Chen S, Hou Y. Understanding the thermal conductivity of Diamond/copper composites by first-principles calculations. Carbon. 2019;148:249–57.
92. Matsubara H, Kikugawa G, Bessho T, Ohara T. Evaluation of thermal conductivity and its structural dependence of a single nanodiamond using molecular dynamics simulation. Diam Relat Mater. 2020;102:107669.
93. Song N, Wang P, Cao D, Wang Z, Ding P. Enhanced thermal conductivity of PP hybrid films induced by filler orientation and laminated structure. J Mater Sci. 2022;57(4):2540–9.
94. Zhang Y, Wang W, Zhang F, Huang L, Dai K, Li C, Liu D, Sun Y, Ren D, Wu J. Micro-diamond assisted bidirectional tuning of thermal conductivity in multifunctional graphene nanoplatelets/nanofibrillated cellulose films. Carbon. 2022;189:265–75.
95. Gu T, Sun D-x, Qi X-d, Yang J-h, Zhao C-s, Lei Y-z, Wang Y. Synchronously enhanced thermal conductivity and heat resistance in Poly (l-lactide)/graphene nanoplatelets composites via constructing stereocomplex crystallites at interface. Compos Part B: Eng. 2021;224:109163.
96. Li X, Wang H, Yang X, Zhang X, Ma B. Simple in situ synthesis of SiC nanofibers on graphite felt as a scaffold for improving performance of paraffin-based composite phase change materials. RSC Adv. 2022;12(2):878–87.
97. Wu X, Tang B, Chen J, Shan L, Gao Y, Yang K, Wang Y, Sun K, Fan R, Yu J. Epoxy composites with high cross-plane thermal conductivity by constructing all-carbon multidimensional carbon fiber/graphite networks. Compos Sci Technol. 2021;203:108610.
98. Guo Y, Wang S, Ruan K, Zhang H, Gu J. Highly thermally conductive carbon nanotubes pillared exfoliated graphite/polyimide composites. Npj Flex Electron. 2021;5(1):16.
99. Li Y, Tian X, Yang W, Li Q, Hou L, Zhu Z, Tang Y, Wang M, Zhang B, Pan T. Dielectric composite reinforced by in-situ growth of carbon nanotubes on Boron nitride nanosheets with high thermal conductivity and mechanical strength. Chem Eng J. 2019;358:718–24.

100. Li C, Yang Z, Zhang X, Ru Y, Gao D, Wu D, Sun J. Ultrasonic-assisted method for the Preparation of carbon nanotube-graphene/polydimethylsiloxane composites with integrated thermal conductivity, electromagnetic interference shielding, and mechanical performances. Int J Mol Sci. 2022;23(23):15007.
101. Liu S, Lan M, Li G, Piao Y, Ahmoum H, Wang Q. Breaking the tradeoff among thermoelectric parameters by multi composite of porosity and CNT in AZO films. Energy. 2021;225:120320.
102. Choi M, An J, Lee H, Jang H, Park JH, Cho D, Song JY, Kim SM, Oh M-W, Shin H. High figure-of-merit for ZnO nanostructures by interfacing lowly-oxidized graphene quantum Dots. Nat Commun. 2024;15(1):1996.
103. Sreekumar S, Ganguly A, Khalil S, Chakrabarti S, Hewitt N, Mondol JD, Shah N. Thermo-optical characterization of novel MXene/Carbon-dot hybrid nanofluid for heat transfer applications. J Clean Prod. 2024;434:140395.
104. Wei Z, Gong P, Kong X, Li M, Cheng J, Zhou H, Li D, Ye Y, Lu X, Yu J. Enhanced thermal conductivity of nanodiamond nanosheets/polymer nanofiber composite films by uniaxial and coaxial electrospinning: implications for thermal management of nanodevices. ACS Appl Nano Mater. 2023;6(10):8358–66.
105. Li L, Qin Y, Wang H, Li M, Song G, Wu Y, Wei X, Ali Z, Yi J, Song S. Improving thermal conductivity of Poly (vinyl alcohol) composites by using functionalized nanodiamond. Compos Commun. 2021;23:100596.
106. Gong P, Li L, Fu G-e, Shu S, Li M, Wang Y, Qin Y, Kong X, Chen H, Jiao C. Highly flexible cellulose nanofiber/single-crystal nanodiamond flake heat spreader films for heat dissipation. J Mater Chem C. 2022;10(33):12070–9.
107. Lee JS, Mun JH, Joo S, Lee SU, Kim MI. The thermal conductivity characteristics of carbon block with Nano-Diamond. Appl Chem Eng. 2023;34(6):608–12.
108. Zhang C, Guo Q, Tong Z, Chen S, Mao Z, Yu Y. Thin film nanoarchitectonics of layer-by-layer assembly with reduced graphene oxide on intraocular lens for photothermal therapy of posterior capsular opacification. J Colloid Interface Sci. 2022;619:348–58.
109. Zou Y, He Q, Wang S, Zou F, Lu X, Sun Z, Li L. Fabrication of graphene oxide/poly (L-lactide-co-ε-caprolactone) nanocomposite with NIR light-induced shape memory effect and antibacterial properties. J Polym Res. 2023;30(6):206.
110. Henriques PC, Pereira AT, Bogas D, Fernandes JR, Pinto AM, Magalhaes FD, Goncalves IC. Graphene films irradiated with safe low-power NIR-emitting diodes kill multidrug resistant bacteria. Carbon. 2021;180:10–21.
111. Shi W, Han Q, Wu J, Ji C, Zhou Y, Li S, Gao L, Leblanc RM, Peng Z. Synthesis mechanisms, structural models, and photothermal therapy applications of top-down carbon Dots from carbon powder, graphite, graphene, and carbon nanotubes. Int J Mol Sci. 2022;23(3):1456.
112. Ovando-Medina VM, Escobar-Villanueva AG, Martínez-Gutiérrez H, González-Ortega O. Interfacial photothermal water evaporator based on nanoporous microwave-expanded graphite and coconut waste fibers@ recycled polystyrene as substrate. Int J Energy Res. 2020;44(13):10878–93.
113. Cao G, Li Y, Qi Y, Qiao Y, He J, Zhang H, Cui W, Zhou M. NIR-responsible and optically monitored nanoparticles release from electrospinning fibrous matrices. Mater Today Adv. 2020;6:100044.
114. Meng Y, Wang C, Song L, Su Z, Jiang Y, Lian Y, Bai G, Fan Q. Composite films based on Bi2Se3 nanosheets and carbon nanotubes with photothermal and photodynamic functions for synergistic treatment. Mater Design. 2023;233:112201.
115. Chen X, Wang L, Zhang D, Bu N, Liu W, Wu Z, Mu R, Tan P, Zhong Y, Pang J, Enhancing Strawberry Freshness. Multifunction Sustainable Films Utilizing Two Types of Modified Carbon Nanotubes for Photothermal Food Packaging, ACS Applied Materials & Interfaces (2024).
116. Liu Y, Xu B, Lu M, Li S, Guo J, Chen F, Xiong X, Yin Z, Liu H, Zhou D. Ultrasmall Fe-doped carbon Dots nanozymes for photoenhanced antibacterial therapy and wound healing. Bioactive Mater. 2022;12:246–56.
117. Luo Q, Liu P, Fu L, Hu Y, Yang L, Wu W, Kong X-Y, Jiang L, Wen L. Engineered cellulose nanofiber membranes with ultrathin low-dimensional carbon material layers for photothermal-enhanced osmotic energy conversion. ACS Appl Mater Interfaces. 2022;14(11):13223–30.
118. Hu L, Sun W, Tang Y, Li S, Zhang B, Sun X, Ji W, Ma L, Deng H, Han S. Photothermal effect enhancing graphene quantum Dots/semiconducting polymer/nanozyme-mediated cancer catalytic therapy. Carbon. 2021;176:148–56.
119. Li Y, Kong J, Zhao H, Liu Y. Synthesis of multi-stimuli responsive Fe3O4 coated with diamonds nanocomposite for magnetic assisted chemo-photothermal therapy. Molecules. 2023;28(4):1784.
120. Wang P, Hou Z, Wang Z, Luo X. Multifunctional therapeutic nanodiamond hydrogels for Infected-Wound healing and cancer therapy. ACS Appl Mater Interfaces. 2024;16(8):9656–68.
121. Mahapatra SS, Yadav SK, Lee BH, Cho JW. Nanodiamond-grafted hyperbranched polymers anchored with carbon nanotubes: mechanical, thermal, and photothermal shape-recovery properties. Polymer. 2019;160:204–9.
122. Han M, Sun W, Chen Y, Li H. Fabrication of a photothermal antibacterial platform for bacterial infectious skin wound healing: a review. Mol Syst Des Eng. 2024;9(8):800–13.
123. Liu H, Xing F, Zhou Y, Yu P, Xu J, Luo R, Xiang Z, Maria Rommens P, Liu M, Ritz U. Nanomaterials-based photothermal therapies for antibacterial applications. Mater Design. 2023;233:112231.
124. Parreño RP, Liu Y-L, Beltran AB. Effect on thermal stability of microstructure and morphology of thermally-modified electrospun fibers of polybenzoxazines (PBz) blended with sulfur copolymers (SDIB). RSC Adv. 2021;11(17):10002–9.
125. Cui X, Ruan Q, Zhuo X, Xia X, Hu J, Fu R, Li Y, Wang J, Xu H. Photothermal nanomaterials: A powerful Light-to-Heat converter. Chem Rev. 2023;123(11):6891–952.
126. Wang X, Cao W, Su Z, Zhao K, Dai B, Gao G, Zhao J, Zhao K, Wang Z, Sun T. Fabrication of high thermal conductivity Nanodiamond/aramid nanofiber composite films with superior multifunctional properties. ACS Appl Mater Interfaces. 2023;15(22):27130–43.
127. Song N, Jin Y, Jiao D, Wang Q, Wang Z, Ding P. Hydrophobic nanofiber Cellulose-Graphene films for High-Performance thermal management applications. ACS Appl Nano Mater. 2024;7(5):4742–52.
128. Jiao E, Wu K, Liu Y, Zhang H, Zheng H, Xu C-a, Shi J, Lu M. Nacre-like robust cellulose nanofibers/mxene films with high thermal conductivity and improved electrical insulation by nanodiamond. J Mater Sci. 2022;57(4):2584–96.
129. Song N, Cui S, Hou X, Ding P, Shi L. Significant enhancement of thermal conductivity in nanofibrillated cellulose films with low mass fraction of nanodiamond. ACS Appl Mater Interfaces. 2017;9(46):40766–73.
130. Terracciano M, Tramontano C, Moretta R, Miranda B, Borbone N, De Stefano L, et al. Protein-modified porous silicon optical devices for biosensing, Porous Silicon for Biomedical Applications, Elsevier. 2021, pp. 113–48.
131. Puntervold T, Strand S, Mamonov A, Piñerez IDT. Enhanced oil recovery by Smart Water injection in sandstone reservoirs, Recovery Improvement, Elsevier2023, pp. 109–184.
132. Siddiqa A, Majid A, Saira F, Farooq S, Qureshi R, Qaisar S. Nanodiamond embedded polyaniline/polyvinylidene fluoride nanocomposites as microfiltration membranes for removal of industrial pollution. RSC Adv. 2023;13(42):29206–14.
133. Wong CCQ, Tomura K, Yamamoto O. Wound healing performance in a moist environment of crystalline glucose/mannose film as a new dressing material using a rat model: comparing with Medical-Grade wound dressing and alginate. Pharmaceuticals. 2023;16(11):1532.
134. Olăreț E, Drăgușin D-M, Serafim A, Lungu A, Șelaru A, Dobranici A, Dinescu S, Costache M, Boerașu I. Vasile, electrospinning fabrication and cytocompatibility investigation of nanodiamond particles-gelatin fibrous tubular scaffolds for nerve regeneration. Polymers. 2021;13(3):407.
135. Narla A, Fu W, Kulaksizoglu A, Kume A, Johnson BR, Raman AS, Wang F, Magasinski A, Kim D, Kousa M. Nanodiamond-Enhanced nanofiber separators for High-Energy Lithium-Ion batteries. ACS Appl Mater Interfaces. 2023;15(27):32678–86.
136. Houshyar S, Padhye R, Shanks RA, Nayak R. Nanodiamond fabrication of superhydrophilic wool fabrics. Langmuir. 2019;35(22):7105–11.
137. Park H, Patil TV, Lee J, Kim H, Cho SJ, Lim KT. NIR-activated catechol-functionalized nanodiamond nanofibers for accelerating on-demand MRSA and E. coli biofilm eradication. J Biol Eng. 2025;19(1):2.
138. Jiang Z, Zheng Z, Yu S, Gao Y, Ma J, Huang L, Yang L. Nanofiber Scaffolds as Drug Delivery Syst Promoting Wound Healing Pharm. 2023;15(7):1829.
139. Zheng Q, Xi Y, Weng Y. Functional electrospun nanofibers: fabrication, properties, and applications in wound-healing process. RSC Adv. 2024;14(5):3359–78.
140. Rajabifar N, Rostami A, Afshar S, Mosallanezhad P, Zarrintaj P, Shahrousvand M, Nazockdast H. Wound dressing with electrospun Core-Shell nanofibers: from material selection to synthesis. Polymers. 2024;16(17):2526.
141. Zhang J, Li Y, Sheng G. Nanodiamond-Reinforced polyurethane micro/nanofiber membrane for UV protection in multifunctional textiles. ACS Appl Nano Mater. 2024;7(11):12323–33.
142. Jahani M, Asefnejad A, Al-Musawi MH, Mohammed AA, Al-Sudani BT, Hameed Al-bahrani M, Kadhim NA, Shahriari-Khalaji M, Valizadeh H, Sharifianjazi F, Mehrjoo M, Tavamaishvili K, Tavakoli M. Antibacterial and wound

healing stimulant nanofibrous dressing consisting of soluplus and soy protein isolate loaded with mupirocin. Sci Rep. 2024;14(1):26397.
143. Neuhoferova E, Kindermann M, Buzgo M, Vocetkova K, Panek D, Cigler P, Benson V. Topical SiRNA therapy of diabetic-like wound healing. J Mater Chem B. 2025;13(3):1037–51.
144. Xu J, Chow EK-H. Biomedical applications of nanodiamonds: from drug-delivery to diagnostics. SLAS Technol. 2023;28(4):214–22.
145. Joudeh N, Linke D. Nanoparticle classification, physicochemical properties, characterization, and applications: a comprehensive review for biologists. J Nanobiotechnol. 2022;20(1):262.
146. Qian Y, Cheng Y, Ouyang Y, Yuan W, Fan C. Multilayered spraying and gradient dotting of nanodiamond–polycaprolactone guidance channels for restoration of immune homeostasis. NPG Asia Mater 11 (2019).
147. Ahn GY, Ryu T-K, Choi YR, Park JR, Lee MJ, Choi S-W. Fabrication and optimization of Nanodiamonds-composited Poly (ε-caprolactone) fibrous matrices for potential regeneration of hard tissues. Biomaterials Res. 2018;22(1):16.
148. Cao L, Hou Y, Lafdi K, Urmey K. Fluorescent composite scaffolds made of nanodiamonds/polycaprolactone. Chem Phys Lett. 2015;641:123–8.
149. Price JC, Levett SJ, Radu V, Simpson DA, Barcons AM, Adams CF, Mather ML. Quantum sensing in a Physiological-Like cell niche using fluorescent nanodiamonds embedded in electrospun polymer nanofibers. Small. 2019;15(22):1900455.
150. Brady MA, Renzing A, Douglas TE, Liu Q, Wille S, Parizek M, Bacakova L, Kromka A, Jarosova M, Godier G. Development of composite Poly (lactide-co-glycolide)-nanodiamond scaffolds for bone cell growth. J Nanosci Nanotechnol. 2015;15(2):1060–9.
151. Şelaru A, Drăguşin D-M, Olăreţ E, Serafim A, Steinmüller-Nethl D, Vasile E, Iovu H, Stancu I-C, Costache M, Dinescu S. Fabrication and biocompatibility evaluation of nanodiamonds-gelatin electrospun materials designed for prospective tissue regeneration applications. Materials. 2019;12(18):2933.
152. Houshyar S, Sarker A, Jadhav A, Kumar GS, Bhattacharyya A, Nayak R, Shanks RA, Saha T, Rifai A, Padhye R. Polypropylene-nanodiamond composite for hernia mesh. Mater Sci Engineering: C. 2020;111:110780.
153. Steinerova M, Matejka R, Stepanovska J, Filova E, Stankova L, Rysova M, Martinova L, Dragounova H, Domonkos M, Artemenko A. Human osteoblast-like SAOS-2 cells on submicron-scale fibers coated with nanocrystalline diamond films. Mater Sci Engineering: C. 2021;121:111792.
154. Kotteeswaran V, Saravanakumar M, Alexander RM, Nair RS, Ramnath KM. Advancement of nanofibers in wound healing: A review. Biomedical Pharmacol J. 2024;17(3):1407–31.
155. Partovi A, Khedrinia M, Arjmand S. Ranaei Siadat, electrospun nanofibrous wound dressings with enhanced efficiency through carbon quantum Dots and citrate incorporation. Sci Rep. 2024;14(1):19256.
156. Ren S, Guo S, Yang L, Wang C. Effect of composite biodegradable biomaterials on wound healing in diabetes. Front Bioeng Biotechnol. 2022;10:1060026.
157. Li R, Vedelaar T, Mzyk A, Morita A, Padamati SK, Schirhagl R. Following polymer degradation with nanodiamond magnetometry. ACS Sens. 2022;7(1):123–30.
158. Mahdavi M, Mahmoudi N, Rezaie Anaran F, Simchi A. Electrospinning of Nanodiamond-Modified polysaccharide nanofibers with Physico-Mechanical properties close to natural skins. Mar Drugs 14(7) (2016).
159. Gong H, Anasori B, Dennison CR, Wang K, Kumbur EC, Strich R, Zhou JG. Fabrication, biodegradation behavior and cytotoxicity of Mg-nanodiamond composites for implant application. J Mater Sci Mater Med. 2015;26(2):110.
160. Melnikov PV, Alexandrovskaya AY, Naumova AO, Popova NM, Spitsyn BV, Zaitsev NK, Yashtulov NA. Modified nanodiamonds as a means of polymer surface functionalization. From fouling suppression to biosensor design. Nanomaterials. 2021;11(11):2980.
161. Belouhova MV, Yotinov ID, Topalova YI. Nanodiamonds improve Amaranth biodegradation in a lab-scale biofilter. Biotechnol Biotechnol Equip. 2023;37(1):317–28.
162. Vittorazzi C, Endringer DC, Andrade TUd, Scherer R, Fronza M. Antioxidant, antimicrobial and wound healing properties of Struthanthus vulgaris. Pharm Biol. 2016;54(2):331–7.
163. Comino-Sanz IM, López-Franco MD, Castro B, Pancorbo-Hidalgo PL. The role of antioxidants on wound healing: A review of the current evidence. J Clin Med 10(16) (2021).
164. Bolshakova O, Lebedev V, Mikhailova E, Zherebyateva O, Aznabaeva L, Burdakov V, Kulvelis Y, Yevlampieva N, Mironov A, Miroshnichenko I, Sarantseva S. Fullerenes on a nanodiamond platform demonstrate antibacterial activity with low cytotoxicity. Pharmaceutics 15(7) (2023).
165. Li F-K, Zhao W-B, Wang Y, Huang W-T, Ku Y-L, Liu H, Guo R, Yu H-H, Liu K-K, Shan C-X. Cationic engineered nanodiamonds for efficient antibacterial surface with strong wear resistance. Nano Res. 2024;17(3):939–48.
166. Chang B-M, Pan L, Lin H-H, Chang H-C. Nanodiamond-supported silver nanoparticles as potent and safe antibacterial agents. Sci Rep. 2019;9(1):13164.
167. Wehling J, Dringen R, Zare RN, Maas M, Rezwan K. Bactericidal activity of partially oxidized nanodiamonds. ACS Nano. 2014;8(6):6475–83.
168. Wu X, Li W, Herlah L, Koch M, Wang H, Schirhagl R. M.K. Włodarczyk-Biegun, melt electrowritten poly-lactic acid/nanodiamond scaffolds towards wound-healing patches. Mater Today Bio. 2024;26:101112.
169. Khalid A, Bai D, Abraham AN, Jadhav A, Linklater D, Matusica A, Nguyen D, Murdoch BJ, Zakhartchouk N, Dekiwadia C. Electrospun nanodiamond–silk fibroin membranes: A multifunctional platform for biosensing and wound-healing applications. ACS Appl Mater Interfaces. 2020;12(43):48408–19.
170. Conceição K, de Andrade VM, Trava-Airoldi V, Capote G. High antibacterial properties of DLC film doped with nanodiamond. Surf Coat Technol. 2019;375:395–401.
171. Shen Y, Li Y, Wen Y, Yang R, Liu Y, Feng X, et al. Investigations into the antimicrobial behavior and cytotoxicity of purified detonation diamond nanoparticles and their assembled micro-/nano-structured films. Mater Lett. 2024;363:136294.
172. Zhang X, Wang Y, Gao Z, Mao X, Cheng J, Huang L, Tang J. Advances in wound dressing based on electrospinning nanofibers. J Appl Polym Sci. 2024;141(1):e54746.
173. Guarino V, Cruz-Maya I, Reineck P, Abe H, Ohshima T, Fox K, Greentree AD, Gibson BC, Ambrosio L. Fluorescent nanodiamonds embedded in poly-ε-caprolactone fibers as biomedical scaffolds. ACS Appl Nano Mater. 2020;3(11):10814–22.
174. Augustine R, Kalva SN, Dalvi YB, Varghese R, Chandran M, Hasan A. Air-jet spun tissue engineering scaffolds incorporated with diamond nanosheets with improved mechanical strength and biocompatibility. Colloids Surf B. 2023;221:112958.
175. Houshyar S, Kumar GS, Rifai A, Tran N, Nayak R, Shanks RA, Padhye R, Fox K, Bhattacharyya A. Nanodiamond/poly-ε-caprolactone nanofibrous scaffold for wound management. Mater Sci Engineering: C. 2019;100:378–87.

Publisher's note